

**DEVELOPING AND VERIFYING AN UNOBTRUSIVE SURGICAL
NAVIGATION PROCEDURE FOR TOTAL SHOULDER
ARTHROPLASTY**

by

ODED AMINOV

B.Sc., The University of British Columbia, 2018

A THESIS SUBMITTED IN PARTIAL FULFILLMENT OF THE REQUIREMENTS FOR
THE DEGREE OF

MASTER OF APPLIED SCIENCE

in

THE FACULTY OF GRADUATE AND POSTDOCTORAL STUDIES

(Biomedical Engineering)

THE UNIVERSITY OF BRITISH COLUMBIA

(Vancouver)

February 2021

© Oded Aminov, 2021

The following individuals certify that they have read, and recommend to the Faculty of Graduate and Postdoctoral Studies for acceptance, the thesis entitled:

Developing and verifying an unobtrusive surgical navigation procedure for total shoulder arthroplasty.

submitted by Oded Aminov in partial fulfillment of the requirements for

the degree of Master of Applied Science

in Biomedical Engineering

Examining Committee:

Dr. Antony Hodgson, Mechanical Engineering, University of British Columbia

Supervisor

Dr. William Regan, Department of Orthopedics, University of British Columbia

Supervisory Committee Member

Dr. Josh W. Giles, Mechanical Engineering, University of Victoria

Supervisory Committee Member

Dr. David Wilson, Department of Orthopedics, University of British Columbia

Additional Examiner

Abstract

Glenoid implantation accuracy in total shoulder arthroplasty (TSA) has been significantly improved by the use of surgical navigation systems. Despite its benefits, surgical navigation has not been widely implemented into TSA procedures. Based on feedback from orthopaedic surgeons, we believe this lack of adoption is due to the obtrusiveness of the optical trackers that protrude into the surgeon's workspace. Furthermore, these systems require time to calibrate during surgery and offer limited options for camera placement, which may cause inconvenience intra-operatively. To tackle these challenges, we developed and assessed a new TSA protocol based on a less-intrusive dental navigation system developed by Navigate Surgical Technologies (NST). Our proposed system consists of laser-engraved surgical drills which are calibrated once when manufactured, and do not require calibration in the operating room. Similarly, we present a design for a substantially smaller bone tracker that can be tracked from almost all directions due to its curved pattern design.

To assess our system's performance, we modified the NST software to support guidance of a TSA procedure. We then conducted a user study in which three participants used the system to drill multiple holes in a glenoid model. Using a CMM (coordinate measuring machine), we determined the resulting trajectory of the surgical drill and compared this to the pre-planned trajectory. Since we used a model glenoid rather than anatomical specimens, we were unable to test a realistic registration process, so were limited to reporting precision only and not accuracy. We found that our system's targeting precision was markedly lower than the end-to-end precision achieved by the main commercially-available TSA navigation system (ExactechGPS) - < 1 degree in standard deviation for both version and inclination in the targeting phase compared with 2.8/4.8 degrees end-to-end for Exactech. Our system's translational precision in locating the entry hole

was sub-millimetric. The primary implication of this work is that a less obtrusive navigation system for TSA is likely feasible, which could potentially improve the uptake rates of surgical navigation for TSA and thereby potentially improve overall surgical outcomes. These findings justify further development of the system and evaluation on cadaveric specimens.

Lay Summary

Surgical navigation systems are known to improve the results of a shoulder replacement surgery, yet despite their benefits, this technology has not been widely adopted into the clinic. We believe that surgeons are uncomfortable with the large size of the currently available systems, as it may interfere with their workflow and workspace.

We partnered with Navigate Surgical Technologies, a Vancouver-based company that has developed a very small, yet sufficiently accurate, navigation system for the dental market. While their small component design is mandatory for dental surgeries, the reduced size can improve surgeon comfort during orthopedic surgery. Hence, we pursued a project to investigate whether the unique technology behind this dental-grade product can be used successfully in an orthopaedic procedure. We found that we were able to integrate these smaller components into a model-based simulated shoulder replacement surgery and achieve better targeting precision than the overall procedure precision of existing systems.

Preface

All work presented in this thesis is original work conducted by the author, Oded Aminov. The concept of applying the dental tracking technology to Total Shoulder Arthroplasty procedures was proposed by Dr. Antony Hodgson, who provided continuous guidance for methodology, analysis, and thesis writing for this project.

Dr. William Regan provided clinical direction for the project and contributed clinical knowledge that drove the requirement setting process for the system.

Josh Giles provided technical guidance and supervision, and provided insight on methodology that drove the experimental methods.

Andres Medina and Tyler Dodds Provided technical knowledge of the NST system. Tyler additionally provided modifications of the registration and guidance modules, as well as the virtual surgical drill definition which were all used to conduct the surgery.

Table of Contents

Abstract.....	iii
Lay Summary	v
Preface.....	vi
Table of Contents.....	vii
List of Tables	x
List of Figures	xi
List of Abbreviations	xvi
Acknowledgments.....	xvii
Chapter 1: Introduction and Background.....	1
1.1 Total Shoulder Arthroplasty	1
1.2 High Revision Rates in TSA.....	2
1.3 Poor Alignment Causes Increased Revision Rates	3
1.4 Glenoid Implant – The Component That Tends to Fail	5
1.5 Methods Used to Improve Implantation Accuracy	6
1.5.1 Patient Specific Instrumentation (PSI).....	7
1.5.2 Surgical Navigation	8
1.5.3 Accuracy Comparison Chart	10
1.5.4 Benefits and Drawbacks of PSI and Navigation In TSA	12
1.6 Defining the Ideal Navigation System	13
1.7 Proposed Navigation System Design	14
1.8 Summary and Research Objectives.....	15
Chapter 2: Methods – System Development.....	16
2.1 Surgical Context and Process	17
2.1.1 Patient Positioning During Shoulder Arthroplasty.....	17
2.1.2 Conventional TSA Technique	18
2.2 Patient Tracker (PT).....	19

2.3	Fabricated PT- Bone mount.....	21
2.4	Surgical Drill Tracking.....	25
2.4.1	Surgical Drill.....	25
2.4.2	Marker Array.....	26
2.4.3	Marking the Drill.....	29
2.5	Drill Length Measurement.....	30
2.6	Stereo Cameras.....	31
2.7	Binary CT scan.....	32
2.8	Glenoid Implant.....	33
2.9	NST User Interface 2.6 Planning, Registration, and Guidance Modules.....	34
2.9.1	Planning Module.....	35
2.9.2	Registration Module.....	36
2.9.3	Guidance Module.....	39
Chapter 3: Methods – Evaluation Process.....		40
3.1	The Concept.....	40
3.1.1	Drilling Jig Setup.....	41
3.1.2	Plastic Inserts.....	43
3.2	Measuring pins.....	44
3.3	System Setup on Trial Day.....	45
3.3.1	Mock Surgery Instructions.....	47
3.4	Trial Measurements.....	47
3.5	Drilling and Re-insertion Accuracy Tests.....	49
3.6	Comparing Probed Points to Plan.....	50
3.7	Rotating Probed Points to Match the Conventional Axes Layout.....	53
3.8	Calculating Trajectory Angulation.....	54
3.9	Drill Calibration.....	55
3.9.1	Physical Device.....	55
3.9.2	Phantom Test Protocol.....	56
Chapter 4: Results.....		58
4.1	Entry Point Variability.....	58

4.2	Trajectory Angulation Variability.....	58
4.3	Variability Attributable to Aspects of Experiment Design	61
4.4	Assessing Deviations from Plan	63
4.5	Qualitative feedback.....	64
Chapter 5: Discussion.....		65
5.1	Study Limitations.....	66
5.1.1	Tracker Registration	66
5.1.2	Tool Calibration.....	67
5.1.3	Extending Drill Length and Increasing Camera Field of View	68
5.1.4	Plastic Inserts.....	69
5.2	Discussion of System Performance	70
5.3	Recommendations for Moving Towards Clinical Testing	72
5.4	Concluding Remarks.....	73
Bibliography		74
Appendices.....		80
	Appendix A - Measuring Procedural Success.....	80
	Appendix B - Transform Matrix Equations	83
	Appendix C - Representing Probed Points in the I Reference Frame	84
	Appendix D - Python Script Used To Transform Points Through 4x4 Matrices.....	85

List of Tables

- Table 4.1:** Means and standard deviations of the observed entry point location and angulation for the drill trajectory relative to the predefined plan at X_0 , Y_0 , $\theta=0$, $\beta=0$ by participant and 95% confidence intervals for precision..... 61
- Table 4.2:** The standard deviation in measuring the long pin's hole location for all 30 trials. 62
- Table 4.3:** Shows the standard deviation measured for all 30 trials. This variability defines the variability in measurement + drilling. Here we can see that the variability we measured is negligible, especially compared to the other errors. Similarly, the error due to the process of drilling was also found to be modest relative to other sources of error..... 62

List of Figures

- Figure 1.1:** Image of an arthritic anatomical shoulder (left) and a total shoulder replacement (right) in which both the glenoid and humeral components have been implanted in placement of the native surfaces..... 1
- Figure 1.2:** Wear rate of polyethylene glenoid component when articulated against metal humeral heads at different angles of version. Adapted from "Influence of joint kinematics on polyethylene wear in anatomic shoulder joint arthroplasty" by Braun, S., et al., 2018, Journal of Shoulder and Elbow Surgery, 27(9). Copyright [2018] with permission from Elsevier..... 4
- Figure 1.3:** Pegged (left) vs keeled (right) polyethylene glenoid implants for total shoulder arthroplasty (Strauss 2009). Adapted from "The glenoid in shoulder arthroplasty" by Strauss, E. J., et al., 2009, Journal of Shoulder and Elbow Surgery, 18(5). Copyright [2009] with permission from Elsevier. 5
- Figure 1.4:** Trabecular metal implant (left) vs polyethylene implant for total shoulder arthroplasty (Strauss 2009). Adapted from "The glenoid in shoulder arthroplasty" by Strauss, E. J., et al., 2009, Journal of Shoulder and Elbow Surgery, 18(5). Copyright [2009] with permission from Elsevier. 6
- Figure 1.5:** This figure demonstrates a custom PSI shown with surfaces designed to match target areas on the glenoid and scapula. Note the channel provided to guide drilling of the glenoid (red). Adapted from "Patient-specific instrument guidance of glenoid component implantation reduces inclination variability in total and reverse shoulder arthroplasty" by Heylen, S., et al., 2016, Journal of Shoulder and Elbow Surgery, 25(2). Copyright [2016] with permission from Elsevier. 7
- Figure 1.6:** Stereo pair of optical cameras tracking the marker arrays rigidly attached to the surgical tool, and the bone of interest. Adapted from "Navigation in surgery" by Mezger, U., et al., 2013, Langenbecks Archives of Surgery, 398(4), 501-514. Copyright [2013] by Mezger, U., et al. Adapted with permission. 8
- Figure 1.7:** ExactechGPS Shoulder Application system demonstrates a marker array attached to the scapula (Bone Marker) and another marker array attached to the operating tool (Tool Marker). Adapted from "Computer navigation re-creates planned glenoid placement and reduces correction variability in total shoulder arthroplasty: An in vivo case-control study" by Nashikkar, P. S., et al., 2019, Journal of Shoulder and Elbow Surgery, 28(12). Copyright [2019] with permission from Elsevier. 9

Figure 1.8: Surfaces on the glenoid to digitize (left) as prompted by the Exactech UI, and matching of the digitized surfaces to the CT scan (right). Adapted from "Computer navigation re-creates planned glenoid placement and reduces correction variability in total shoulder arthroplasty: An in vivo case-control study" by Nashikkar, P. S., et al., 2019, Journal of Shoulder and Elbow Surgery, 28(12). Copyright [2019] with permission from Elsevier. 10

Figure 1.9: Data compiled from different studies illustrating the accuracy and standard deviations in both version and inclination for TSA procedures carried out using three different kinds of procedures. 1. Gregory (2013), 2. Throckmorton (2015), 3. Villatte (2018), 4. Nashikkar (2019), 5. Wang (2019), 6. Nashikkar (2019) 7. Villatte (2018), 8. Gauci (2016), 9. Throckmorton (2015). * indicates mean absolute deviation reported in a meta-analysis. 11

Figure 1.10: Conventional optical trackers used in navigated surgery (left) compared to the substantially smaller optical trackers developed by NST (right). Adapted from "Real-time intraoperative 3D image intensifier-based navigation in reversed shoulder arthroplasty- analyses of image quality" by Theopold, J., et al., 2019, BMC Musculoskeletal Disorders, 20(1). Copyright [2019] by Theopold, J., et al. Adapted with permission. 14

Figure 2.1: System overview portraying the surgeons and patient layout, and all of the relative positions of the patient tracker, tracked surgical drill, optical cameras, and user interface. 16

Figure 2.2: In the lazy beach chair position, the patient is laid on the operating table with the thorax angled between 30-40 degrees from the horizontal. The shoulder is situated at the edge of the operating table, with the arm being left free to move. (Adapted from Matsen FA III, Lippitt SB. Shoulder Surgery: Principles and Procedures. Philadelphia: Saunders; 2004:514.) 17

Figure 2.3: Navigate Surgical Technologies Inc. patient trackers A (right) and B (left). 20

Figure 2.4: ExactechGPS shoulder Anatomy Tracker (left) compared with our proposed tracker (right). Note that the Exactech tracker is approximately twice as tall as ours. 21

Figure 2.5: Scapula view from two angles rotated 90 degrees relative to one another (left) with a reference to the coracoid process. Intraoperative coracoid process exposure (right) depicts that this bony landmark is the most prominent landmark available. The right most image matches the orientation of the leftmost image. 22

Figure 2.6: Initial prototype of PT-Bone mount with NST tracker attached. CAD design (left), fabricated mount (middle and right). 23

Figure 2.7: Patient tracker rigidly attached onto the coracoid process of the scapula by means of our custom designed PT-Bone Mount. The tracker is positioned similarly to how it would be used in surgery. A side view of the setup (left) shows the apparatus mounted onto a left shoulder. The image on the right shows the camera perspective of the patient tracker when the cameras are located near the head of the patient..... 23

Figure 2.8: Computer rendering of the final prototype of the PT-Bone Mount illustrating both top and bottom surfaces. This mount will accommodate PT A for left shoulder surgeries and PT B for right shoulder surgeries..... 24

Figure 2.9: CONMED HALL 50 surgical drill (left), along with the 3D CAD model derived from measurements made on the drill (right). 26

Figure 2.10: 2D marker array overlaid onto the barrel of the surgical drill..... 27

Figure 2.11: Cross section of drill barrel. Mathematical computations for translating the 2D planar marker array into the 3D cylindrical coordinate system. 28

Figure 2.12: Marker array wrapped around drill barrel 28

Figure 2.13: NST surgical handpiece with laser engraved marker array 29

Figure 2.14: Marker array printed on sticker (left) and later attached to the barrel surface of the drill (right)..... 30

Figure 2.15: Laser engraved dot on NST patient tracker, used to calibrate the drill length offset. 30

Figure 2.16: Point Grey FL3-U3-32S2M-CS cameras mounted onto the NST stereo camera mount made of a rigid aluminum construction, acting as both a heat sink and mechanical mount..... 31

Figure 2.17: Binary simulated CT scan (below) generated from a .STL mesh body file (above) using Slicer 3D. 32

Figure 2.18: Resulting .OBJ mesh body for the glenoid implant generated from a DICOM file from a CT scan. The origin is centered on the top of the central implant peg with the Z axis aligned with the axis of the central peg..... 34

Figure 2.19: Resulting single piece glenoid implant component (green) which incorporates both the dental implant (grey) and dental crown (white). 35

Figure 2.20: Glenoid component imported into the user interface is shown during the planning phase, and is manually manipulated relative to the CT scan of the scapula model..... 36

Figure 2.21: Reference frames associated with registration of the patient tracker (T) to the bone model (B), by probing three points (purple) on the native glenoid (right), and selecting the same three points in the virtual model (left)..... 38

Figure 2.22: NST UI representing three orthogonal views (top-left, top-right, bottom-left) and the 3D view (bottom right) when both trackers are in view of the cameras.	39
Figure 3.1: SAWBONES scapula bone model in the midst of preparation to be used as our surgical jig.	42
Figure 3.2: Prepared bone model mounted onto a steel block. The steel tube insert is visible in the glenoid fossa at top.	43
Figure 3.3: 22mm length prepared Delrin specimen, marked with blue marker for proper orientation.	44
Figure 3.4: Custom made measuring pins with a stem machined to $4.4\text{mm} \pm 0.1\text{mm}$	45
Figure 3.5: Surgical system setup on day of the mock trials, with the attending orthopaedic surgeon holding the drill. The cameras were mounted on the back of the monitor mount, looking down at the surgical drill and patient tracker. The drilling jig was mounted vertically on a vise which was clamped down to the table.	46
Figure 3.6: The uncovered drilling jig (left) and the glenoid surface covered with plasticine (right) in order to prevent the user from using visual cues related to the plastic insert and tube when choosing the drill entry point.	47
Figure 3.7: The seven points indicated in red were the points probed on the bone model to later be used with the ICP. These were selected in accordance with minimum constraint theory to provide reliable and repeatable registrations. The green dots represent the points measured for the long and short pins of a specific trial.	48
Figure 3.8: The drilling jig was mounted on a CNC machine holding a manual 3 axis probe (Haimer 80.365.30.FHN Universal FH 3D Sensor), and was used to find the center of the holes located at the top of the measurement pins by probing and finding the middle point between the x+ and x- limits, as well as y+ and y-. The ball was then plunged down to ensure proper seating on the rim.	49
Figure 3.9: Overview of project reference frames P, S, C, and I, as well as the transform matrices derived and utilized (Tsp, Tcs, Tic).	51
Figure 3.10: Drilling orientation during the mock trials (left) had the implant reference frame oriented such that the positive y-axis was directed in the anatomically superior direction. While probing (right) the implant reference frame was rotated 90° , such that the positive x-axis was directed in the anatomically superior direction.	54

Figure 3.11: The trigonometry used to compute the angles θ and β by considering the offset between the origin and the point probed on the long pin. The two images above are rotated 90 degrees from one another, used to compute inclination (left) and version (right). 55

Figure 3.12: The calibration phantom is a block of stainless steel, with divots machined into it by a high-precision CNC machine at known locations relative to the datum, and later measured on a CMM to confirm accuracy. This device is used to ensure the calibration between a marker array, and the surgical drill which it is rigidly attached to. 56

Figure 3.13: Engineering drawing of the phantom block, with construction specifications for all of the divots relative to the datum. A blue dot represents the divot we probed during our experimentation. 57

Figure 4.1: Entry hole locations of all thirty trials for each participant relative to the pre-plan target of (0, 0). A size reference for the central peg diameter (4.4mm) is shown as a dark blue filled circle, as well as the glenoid dimensions (in grey). The faint blue circle outline in the plots to the right has a radius of 900 microns and illustrates that all trial points for each participant fit within this sub-millimetric area. 59

Figure 4.2: The distribution of executed trajectories (left column) and angular deviations for version and inclination (right column). The top cluster of points in each plot on the left indicates the measured locations of the top pins, while the bottom cluster indicates the measured locations of the entry holes. A size reference for the central peg diameter is indicated by the light orange circles. The faint blue circles have a radius of 3° , which approximates the variability reported for version achieved by the Exactech surgical navigation system (Nashikkar 2019). 60

Figure 4.3: Superior-inferior (top) and anterior-posterior (bottom) offset of drill tip over 941 samples (orange), relative to a predefined point on the calibration phantom (blue). 64

Figure 4.4: Sketch illustrating (exaggerated for effect) the deviation of the assumed drill tip location (orange, based on the central axis of the marker array) relative to the actual location (blue). 64

Figure 5.1: Possible explanation of medial lateral bias in entry hole location (deviations exaggerated for clarity). In the diagrams above, the blue line represents the actual location of the drill, whereas the orange line represents the assumed drill axis based on the center of the cylindrical shell formed by the tracking array. Note that the measured offset corresponds to a rightward displacement of the drilled hole relative to the position indicated on the targeting display. 68

List of Abbreviations

CMM	Coordinate measuring machine
FOV	Field of view
GHOA	Glenohumeral osteoarthritis
HU	Hounsfield levels
ICP	Iterative closest point
IGT	Image-Guided Therapy
NST	Navigate Surgical Technologies Inc.
PSI	Patient specific instrumentation
PT	Patient tracker
THA	Total hip arthroplasty
TKA	Total knee arthroplasty
TSA	Total shoulder arthroplasty
UBC	University of British Columbia
UI	User interface

Acknowledgments

Thank you, Tony, for being an amazing supervisor and mentor. I cannot express my gratitude enough for everything you have done to support me. Without your guidance I would not have been able to get this far. I will forever treasure my time spent at the Surgical Technologies Lab.

Thank you, Josh, for your continuous support with all mathematical, practical, and theoretical matters. Your input expedited the completion of my project, and your prompt support is greatly appreciated.

Thank you, Bill, for your clinical guidance. Despite all of your other commitments you always managed to make time to meet and help me move forward. I truly appreciate your efforts.

Thank you, Andres and Tyler, for your supervision and advice during my time working with NST. I really enjoyed our extended talks about all subjects, and look forward to more of them in the future. You gentlemen have the passion and natural curiosity of true scientists, and I wish you all the best moving forward.

Thank you, Danmei, for always stepping beyond boundaries to ensure that I get the best CT scans possible, and in a timely manner if not immediately.

Thank you, Prash, for sharing your infinite 3D Slicer wisdom. Your extended support has helped me every single time.

Thank you, Dr. David Wilson for agreeing to serve on my examination committee

Chapter 1: Introduction and Background

This chapter introduces the background and motivations which gave rise to our work.

1.1 Total Shoulder Arthroplasty

The shoulder is a ball and socket joint in which the ball, termed the humeral head, articulates against a curved surface on the scapula called the glenoid. Shoulder replacement surgery, also known as total shoulder arthroplasty (TSA), is a generally successful surgical procedure performed when these surfaces are damaged or eroded to the point of discomfort or restrictive range of motion (Schwartz 2014). A total shoulder arthroplasty is a replacement of both the anatomical glenoid and the humeral components of the joint with new synthetic surfaces (Figure 1.1). The eroded glenoid surface is replaced with a smooth polyethylene component, which is often cemented into the specifically prepared glenoid bone (Friedman 2019), while the humeral-sided component replaces the destroyed humeral head.

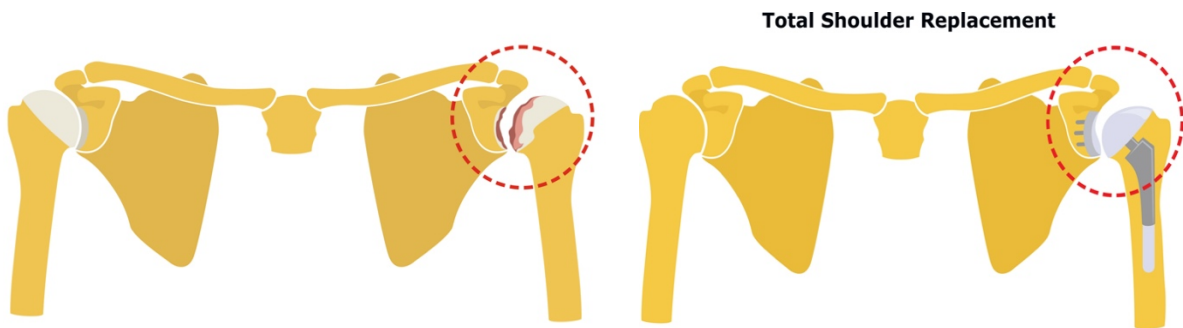


Figure 1.1: Image of an arthritic anatomical shoulder (left) and a total shoulder replacement (right) in which both the glenoid and humeral components have been implanted in place of the native surfaces.

This surgery is popular amongst patients suffering from end-stage glenohumeral osteoarthritis (GHOA), who would otherwise not benefit significantly from non-operative management (Framer 2007).

As the frequency of these cases increases, the demand for total joint replacements is also expected to grow (Healy 2001). More specifically, Boddapati (2017) found that between the years 2000 and 2010, the volume of shoulder arthroplasty procedures had increased by 534%, which is greater than the growth rate of the two most common joint replacement surgeries, total hip arthroplasty (THA) at 182% and knee arthroplasty (TKA) at 231%. With several other studies noting similar results, it is evident that this procedure is gaining traction (Trofa 2014; Jain 2006; Hollatz 2014).

1.2 High Revision Rates in TSA

Since the first case of TSA back in 1893, revision surgeries have been inevitable (Adams 2006). The term ‘revision’ refers to a secondary surgery which is required in order to address issues that arise subsequent to the original surgery. While some factors such as the risk of infection are inherent with any invasive procedure, several other elements are also present contributing to the possibility of a required revision (Page 2018). One of these factors which can be controlled for and consequently reduce the rate of revision surgeries has been found to be the placement accuracy of the glenoid implant (Nashikkar 2019). Inaccurate positioning of the implant can lead to component failure, which mandates a revision surgery in around 11% of cases over a period of 7.5 years (Martin 2005). While this equates to roughly 1.5% annually, it is substantially higher than the values found for total knee arthroplasty (TKA) and total hip arthroplasty (THA). After a follow-up at ten years, Bouras (2015) found a TKA failure rate of roughly 0.7% annually, while Junnila,

(2016) found the failure rate in THA to be 0.6% annually. It is evident that TSA has higher failure rates compared to TKA and THA, suggesting that the joint is either more complex, or there is room for improvement.

With a mean cost of \$13,383 USD for just the services provided by the hospital, it is apparent that reducing the number of revision surgeries can save significant amounts of money for the healthcare system as a whole (Virani 2013). In 2014 alone, there were over 32,700 admissions for an upper extremity reconstruction in the United States (Zmistowski 2018). If revision surgeries could be eliminated, the United States' healthcare system could experience savings of over \$48 million USD annually, not including other indirect costs such as physiotherapy or time off work.

1.3 Poor Alignment Causes Increased Revision Rates

Good positioning of the glenoid implant is essential for the longevity and stability of the shoulder prosthesis, as the lack of accurate placement has been reported to increase aseptic loosening rates of the glenoid implant by 39% (Boshali 2006). Several studies have noted similar results, suggesting that malposition of the glenoid implant, specifically in the anterior-posterior angulation termed version, results in radiographic translucent lines (Farron 2006; Habermeyer 2006; Shapiro 2007), which are often indicators to loss of fixation. More specifically, Hopkins (2004) found that components with improper inclination (Appendix A), which is the inferiorly or superior angulation of the implant, had the highest probability of failure. Similarly, their study found that posteriorly angled glenoid implants, termed retroverted, were most likely to suffer from loosening. These angular deviations result in failure by increasing fracture rates of the cement used to adhere the polyethylene implant to the bone (Yongpravat 2012).

While implant loosening is one major problem, another is glenoid wear. Braun (2018) found that the breakdown rate of the polyethylene implant increases drastically as the version of the implant increases. They conducted their experiment by mounting polyethylene glenoid components onto a complex joint simulator, and tested the wear rate of the implant at 0, 5, and 10 degrees of version (Figure 1.2). It is therefore evident that both these mechanisms (i.e., loosening and wear) can arise from malplacement of the glenoid implant and can lead to decreased longevity of it, resulting in undesirable revision surgeries.

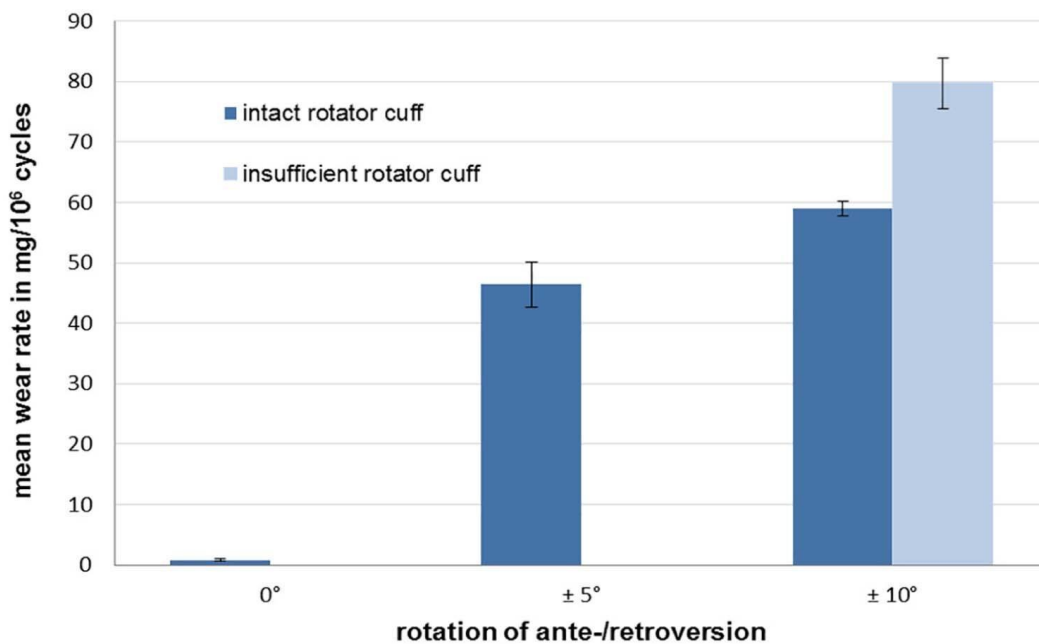


Figure 1.2: Wear rate of polyethylene glenoid component when articulated against metal humeral heads at different angles of version. Adapted from "Influence of joint kinematics on polyethylene wear in anatomic shoulder joint arthroplasty" by Braun, S., et al., 2018, Journal of Shoulder and Elbow Surgery, 27(9). Copyright [2018] with permission from Elsevier.

1.4 Glenoid Implant – The Component That Tends to Fail

In a study that investigated 48 revised shoulders, twenty-nine (60.4%) of the cases were due to glenoid component loosening, and five (10.4%) shoulders were revised due to significant polyethylene glenoid wear (Antuna 2001). Hence it is important to find the component design which is least prone to either of these potential modes of failure. Several implant design and material options are available for surgeons to choose from, so these choices will likely affect both the rates of component loosening and material breakdown.

The first key design option is the shape of the stem used for locking the glenoid to the bone. As shown in Figure 1.3, this shape is either keeled or pegged (Strauss 2009). Lazarus (2002) found that pegged implants yield superior seating into the bone in a postoperative study of 328 patients. Other studies have observed similar results, and the majority of procedures these days use pegged implant designs Gartsman (2005).

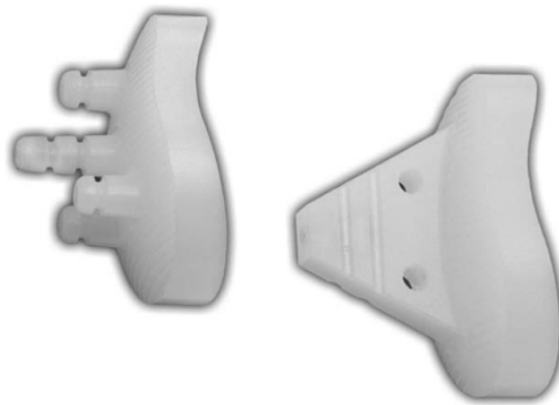


Figure 1.3: Pegged (left) vs keeled (right) polyethylene glenoid implants for total shoulder arthroplasty (Strauss 2009). Adapted from "The glenoid in shoulder arthroplasty" by Strauss, E. J., et al., 2009, *Journal of Shoulder and Elbow Surgery*, 18(5). Copyright [2009] with permission from Elsevier.

The second design choice is flat-backed vs curve-backed implants. After reviewing radiographs from 63 patients, Szabo (2005) found that 65% of curved glenoid implants were perfectly seated, which was superior to the flat back implants at 26%. Finally, there are cemented and non-cemented implants. While non-cemented implants are usually in the form of metal-backed trabecular metal glenoid components, cemented implants are made of polyethylene (Figure 1.4).

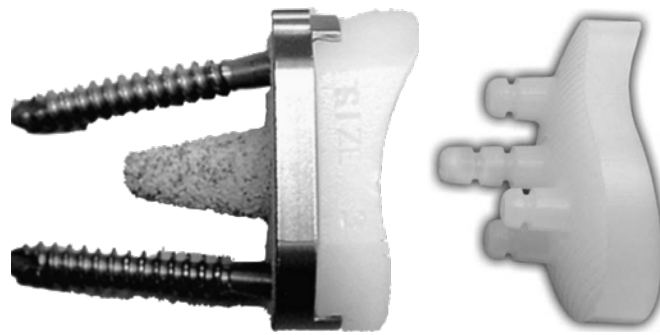


Figure 1.4: Trabecular metal implant (left) vs polyethylene implant for total shoulder arthroplasty (Strauss 2009). Adapted from "The glenoid in shoulder arthroplasty" by Strauss, E. J., et al., 2009, *Journal of Shoulder and Elbow Surgery*, 18(5). Copyright [2009] with permission from Elsevier.

However, after investigating post-operative glenoid loosening in groups with both of the listed implants, Boileau (2002) concluded that the fixation of non-cemented implants is inferior to that of the cemented components. Hence, the cemented polyethylene implant approach is the most common choice for implants today (Merolla 2013).

1.5 Methods Used to Improve Implantation Accuracy

In this section we discuss the two primary methods that have been developed to improve glenoid implantation performance. We then offer a comparison chart of several studies testing the different methods for TSA, and discuss the benefits and drawbacks amongst these systems.

1.5.1 Patient Specific Instrumentation (PSI)

One of the methods which people have used in attempt to improve the implantation accuracy during TSA is known as Patient Specific Instrumentation (PSI). As shown in Figure 1.5, these are bone-mountable guides, manufactured specifically to match the anatomical shape of a patient (Heylen 2016). These guides aid in the surgical process of an operation by providing a channel for a tool to be placed through, guiding the cuts along a predetermined trajectory. In shoulder replacement surgery, PSIs are currently being used to aid with the glenoid implant positioning (Gauci 2016). This is achieved by generating a virtual model of the patient's shoulder using a pre-operative CT scan (Gauci 2016). A planning software such as the Affinis Architec system is then used to generate target drilling channels inside of the PSI, based on the optimal position of the glenoid in both version and inclination (Gauci 2016). Once the planning is complete, the 3D-printed mountable plastic component is fabricated, and put through a sterilization process before being used intraoperatively, once the glenoid has been exposed.



Figure 1.5: This figure demonstrates a custom PSI shown with surfaces designed to match target areas on the glenoid and scapula. Note the channel provided to guide drilling of the glenoid (red). Adapted from "Patient-specific instrument guidance of glenoid component implantation reduces inclination variability in total and reverse shoulder arthroplasty" by Heylen, S., et al., 2016, *Journal of Shoulder and Elbow Surgery*, 25(2). Copyright [2016] with permission from Elsevier.

1.5.2 Surgical Navigation

An alternative approach to PSIs is surgical navigation. A navigation system is a tool used by surgeons during an operation which provides guidance and dynamic feedback for their drilling trajectory (Mezger 2013). Surgical navigation works by employing optically tracked patterns or markers that are observed by a stereo pair of cameras (Figure 1.6). A computer interprets the images from the different viewpoints and calculates the marker or pattern locations in space (Mezger 2013). These optical trackers are rigidly attached to the objects of interest (typically the anatomy being operated on and one or more tools being used in the procedure). A calibration process allows the locations of key features on the anatomy or the tool to be measured relative to the markers or patterns, and relative displacements between objects can be determined and displayed to the user (Mezger 2013). Most conventionally, marker arrays consisting of a minimum of three individual markers are used, as this allows the system to determine the full 3D pose of a tracked object (Mezger 2013).

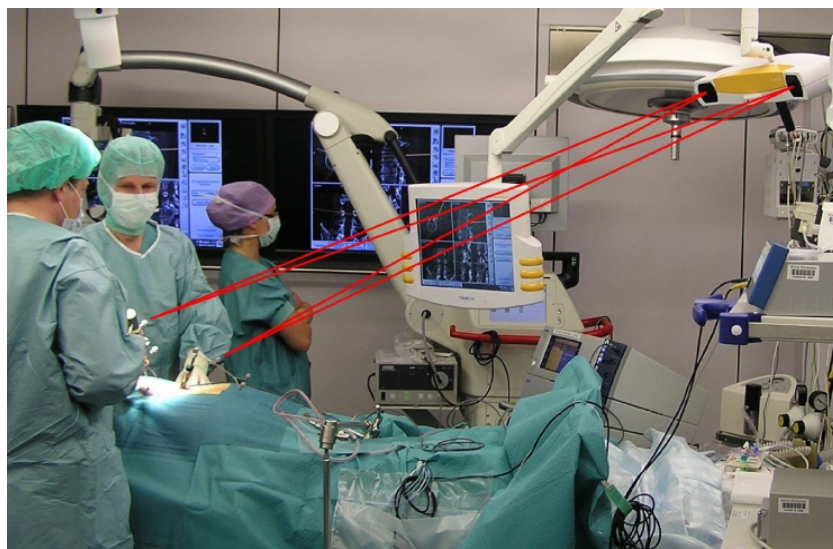


Figure 1.6: Stereo pair of optical cameras tracking the marker arrays rigidly attached to the surgical tool, and the bone of interest. Adapted from "Navigation in surgery" by Mezger, U., et al., 2013, *Langenbecks Archives of Surgery*, 398(4), 501-514. Copyright [2013] by Mezger, U., et al. Adapted with permission.

In the realm of orthopaedic surgery, surgical navigation can be used specifically for arthroplasty procedures by attaching one marker array to the surgical tool, and one array to the bone of interest (Nashikkar 2019). For use in shoulder replacement specifically, one array is typically located on the operating tool, while the other is rigidly attached to the scapula (Figure 1.7)

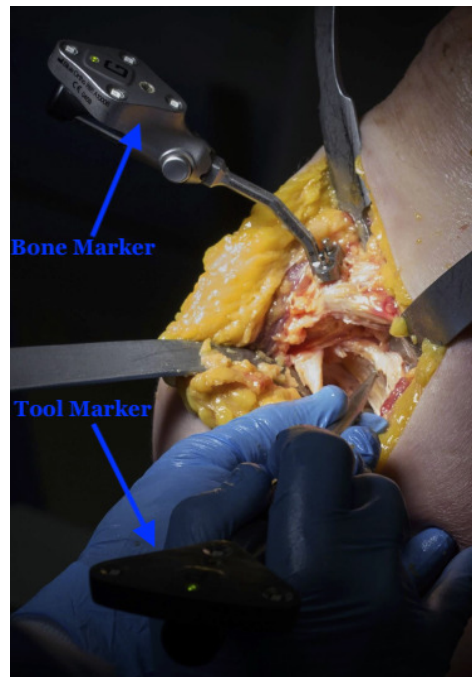


Figure 1.7: ExactechGPS Shoulder Application system demonstrates a marker array attached to the scapula (Bone Marker) and another marker array attached to the operating tool (Tool Marker). Adapted from "Computer navigation re-creates planned glenoid placement and reduces correction variability in total shoulder arthroplasty: An in vivo case-control study" by Nashikkar, P. S., et al., 2019, Journal of Shoulder and Elbow Surgery, 28(12). Copyright [2019] with permission from Elsevier.

The user interface (UI) then displays a representation of the drill's position relative to the scapula, as well as guidance elements such as crosshairs to dynamically portray the current drill position relative to the target. In order to generate the virtual model of the patient which will be displayed in the UI, the pre-operative radiographic images must be imported into the navigation software. In shoulder arthroplasty, pre-operative CT scans are routinely acquired as part of the

diagnostic protocol, so no additional radiation exposure is required to generate the virtual model. Registration then takes place, where landmarks on the actual scapula are aligned with those same landmarks in the virtual scapula derived from the CT scan (Hwang 2019). Figure 1.8 demonstrates how the ExactechGPS Shoulder Application system achieves this registration by means of an additional tracked tool that is swiped on the surface of the glenoid to digitize various landmarks, which are then used to register the two clouds of points (Nashikkar 2019).

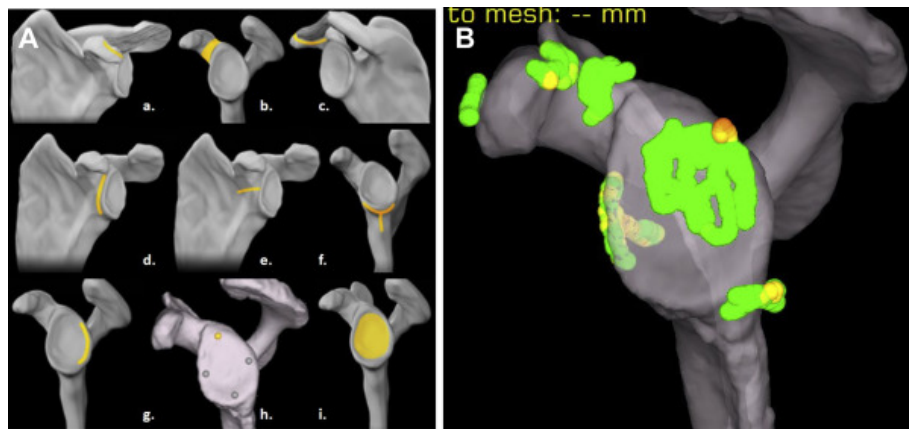


Figure 1.8: Surfaces on the glenoid to digitize (left) as prompted by the Exactech UI, and matching of the digitized surfaces to the CT scan (right). Adapted from "Computer navigation recreates planned glenoid placement and reduces correction variability in total shoulder arthroplasty: An in vivo case-control study" by Nashikkar, P. S., et al., 2019, Journal of Shoulder and Elbow Surgery, 28(12). Copyright [2019] with permission from Elsevier.

The navigated drilling process can now begin, and the surgeon receives immediate feedback on the monitor, for the tool position relative to the intended trajectory, allowing for immediate adjustment (Mezger 2013).

1.5.3 Accuracy Comparison Chart

The graph below represents the post-operative results of the glenoid version and inclination found in nine different studies (Figure 1.9). As described in sections 1.5.1 and 1.5.2, PSI (purple)

and Navigation (green) both portray great accuracy and precision in both version and inclination. More specifically, as presented in Figure 1.9, the reported implantation accuracies for PSI range from three to five degrees in version with standard deviations of five degrees, and two to three degrees in inclination with roughly five degrees in repeatability. Similarly, navigation yields version accuracies of negative one to three degrees in version with standard deviations ranging between two to three degrees, and inclination between zero and five with precision of three to five degrees, based on the studies we are presenting. Conversely, the conventional technique (in orange) is found to have a much larger spread in both accuracy and precision

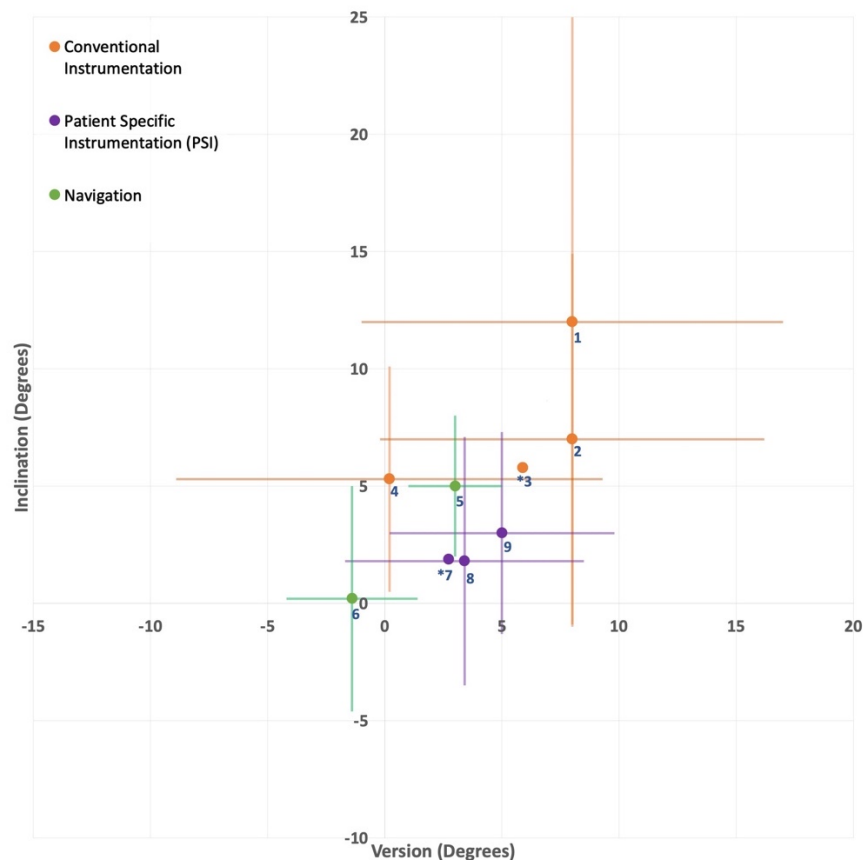


Figure 1.9: Data compiled from different studies illustrating the accuracy and standard deviations in both version and inclination for TSA procedures carried out using three different kinds of procedures. 1. Gregory (2013), 2. Throckmorton (2015), 3. Villatte (2018), 4. Nashikkar (2019), 5. Wang (2019), 6. Nashikkar (2019) 7. Villatte (2018), 8. Gauci (2016), 9. Throckmorton (2015). * indicates mean absolute deviation reported in a meta-analysis.

1.5.4 Benefits and Drawbacks of PSI and Navigation In TSA

While the use of PSIs can improve implant alignment, figuring out how to use them can present a steep learning curve (Gori 2017). Furthermore, good glenoid exposure is essential, which mandates the added step of soft tissue debridement. It is important not to damage any bone in the process, as the guide is designed to sit on the bony structure which was present in the CT prior to the surgery. Incorrect clearing of soft tissues can lead to malplacement of the PSI guide which results in slight glenoid component malplacement (Chow 2016), which as described previously, results in decreased component longevity. Lastly, an added lead time of 10 business days (2 weeks) can be expected for manufacturing the PSI guide (Gauci 2016), while added costs of roughly \$1350USD are also to be incurred (Thienpont 2015). Similar to PSIs, surgical navigation offers improved accuracy and precision for implant placement. While we are only aware of one company, Exactech, who has already released a commercially available navigation system for use in shoulder arthroplasty, their system lives up to the expectation. With an implantation accuracy of $-1.4 \pm 2.8^\circ$ in version and $0.2 \pm 4.8^\circ$ in inclination, the “ExactechGPS Shoulder” offers demonstrably better accuracy for glenoid implantation when compared to the conventional technique (Nashikkar 2019). However, an early evaluation of navigated TSA by Kircher (2009) showed that the time of surgery was increased by 23% (31.5 minutes). This is a problem as it is important to reduce the time of surgery, especially in elderly patients (Wang 2019), in order to reduce the risk of infection. One of the reasons that surgical navigation increases operating time is due to the navigation systems being obtrusive to the surgeon’s workflow and physical space. Wong (2014) suggests that “operating room set-up prior to the surgery must take into account the physical footprint of these large and obtrusive [navigation systems], or risk machine repositioning during the procedure,

thereby disturbing the workflow and increasing operating times”. Wong (2014) further states that surgeons believed these obtrusive parameters lead to reduced accuracy during surgery.

Another drawback for navigation is the initial price of these systems (Bellemans 2009). While we were unable to find the price for a navigation system used in TSA, Watkins (2010) states that the price of a navigation system used for brain surgery (Vector Vision-BrainLAB) is around \$225,000 USD (Watkins, 2010).

1.6 Defining the Ideal Navigation System

As described in section 1.5.4, several obtrusive factors negatively affect surgeon’s willingness to adopt navigation systems. The ideal system would provide all the benefits of the navigation, without any of the obtrusive drawbacks. The existence of such a system would allow a surgeon to pick up a surgical tool and conduct a perfect shoulder replacement surgery regardless of their little to no experience as an upper extremity surgeon. In this ideal scenario, there would be no need for any calibration, there would be no bulky instruments protruding into the surgeon’s workspace, they simply pick up the tools and are immediately guided through to a perfect glenoid implantation. If they chose not to use the guidance, they don’t have to, but it’s there for them if they need it regardless of whether they set it up or not.

A similar concept to the vision described above can be attained by an unobtrusive navigation process, where everything happens as automatically as possible. This would involve integrating the navigation system directly into pre-existing structures in a surgeon’s workflow. An example of such a setup includes cameras mounted in the OR lights, marked trackers are directly on the tools, and laser scanners to detect the glenoid position relative to the anatomy tracker.

1.7 Proposed Navigation System Design

Navigate Surgical Technologies Inc. (NST) is a start-up company that specializes in the development of navigated surgical instruments for dental application. NST offers three advantages with their unique technology, which could bring the experience of navigation in TSA one step closer to the ideal surgery described in section 1.6. Their first advantageous point is in the size of their Patient Trackers (PT). While a small size is a point of parity in the dental market, it serves great convenience in the realm of orthopaedic surgery. The benefit of having smaller trackers is evident in the minimally obtrusive nature of the design, which does not protrude as extensively into the surgeon's working space (Figure 1.10).

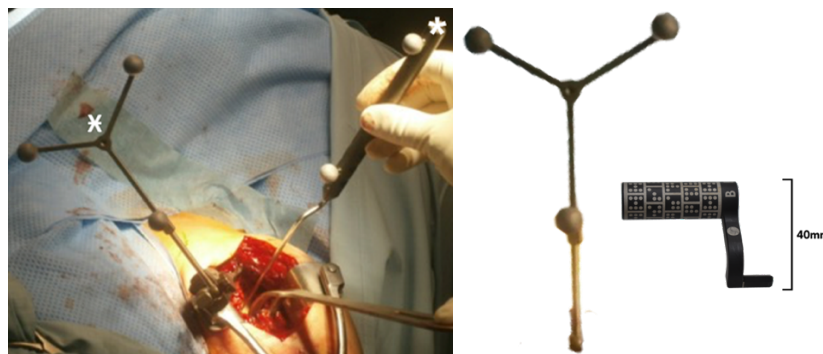


Figure 1.10: Conventional optical trackers used in navigated surgery (left) compared to the substantially smaller optical trackers developed by NST (right). Adapted from "Real-time intraoperative 3D image intensifier-based navigation in reversed shoulder arthroplasty- analyses of image quality" by Theopold, J., et al., 2019, BMC Musculoskeletal Disorders, 20(1). Copyright [2019] by Theopold, J., et al. Adapted with permission.

Their second point of difference is evident in their patented ability to laser engrave the surgical tools directly. Marking the tools eliminates any potential inaccuracies caused by flexion in the coupling between the markers and the tool itself, as per the conventional navigation systems. Furthermore, engraving the tools directly means that calibration can occur once during the manufacturing process, and never again. This makes the process of autoclaving very simple as no

consideration needs to be given to removing the optical markers at the end of surgery, and later dealing with calibration and registration prior to the next operation. Similar to the first point, engraving directly on the tool eliminates the obtrusive markers which would otherwise be moving around with the drill, filling a volume in the surgeon's workspace. Lastly, NST engraves these patterns on a curved surface. The use of a cylindrical marker array instead of a planar version allows the cameras to observe the array from many more angles. One case in which this would be valuable during surgery is in the case that for any reason the cameras need to be moved around the OR to the other side of the patient. While the NST system will continue to track, a system using planar trackers will cease to work. With sub-millimeter accuracy, and a reasonably priced platform which is comparable to or possibly cheaper than existing technologies, this system could soon pay for itself by reducing the costs associated with revision surgeries (Koch 2013). We therefore believe that there is a good application of Navigate Surgical's technology in the medical space.

1.8 Summary and Research Objectives

Despite the demonstrably superior implantation alignment results offered by navigation systems relative to the conventional techniques, surgical navigation systems have not been widely adopted. With strong evidence to suggest that the obtrusiveness of these systems is a major reason for the surgeon's low willingness to adopt, we believe that offering a surgical navigation system which has similar accuracy but reduces obtrusiveness to workflow and physical space will be in greater demand. Hence, our goal is to deliver a demonstration of a total shoulder arthroplasty which uses Navigate Surgical's unobtrusive trackers to perform a sufficiently accurate glenoid implantation.

Chapter 2: Methods – System Development

In this chapter we provide a description of the context and process for the conventional TSA surgery. We then describe the patient trackers, PT-Bone Mount, and surgical drill which we developed, followed by the optical cameras, the user interface, and all UI dependencies such as a binary DICOM and implant CAD files. All of the elements described above are present in Figure 2.1.

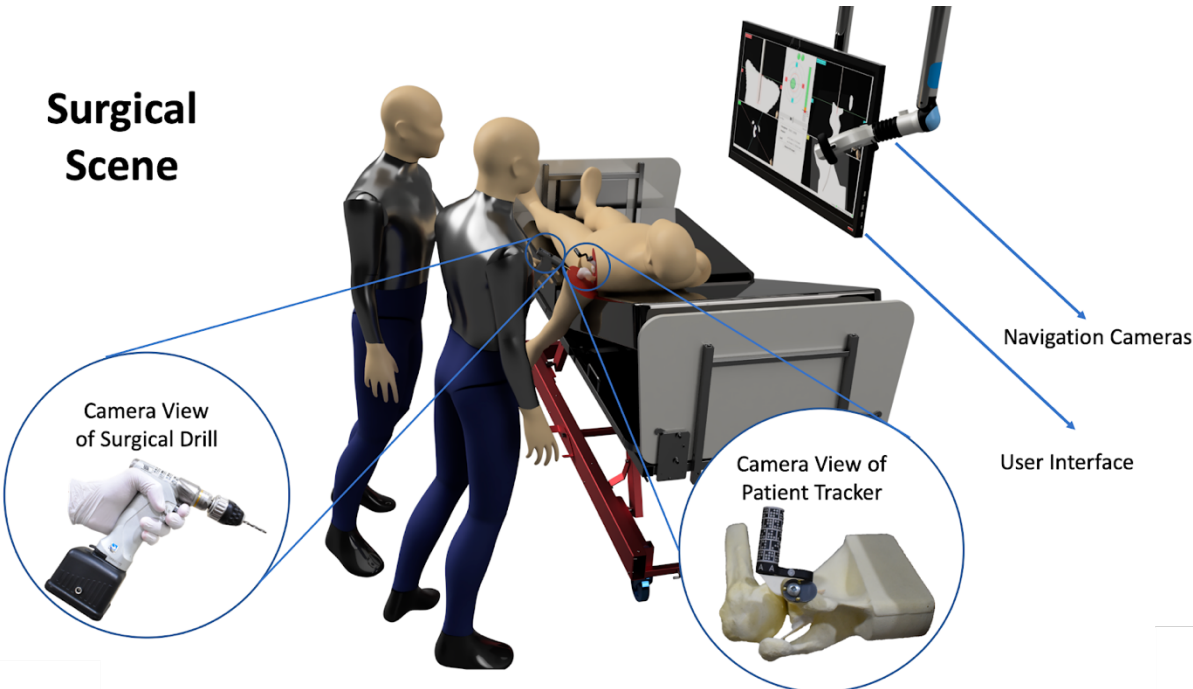


Figure 2.1: System overview portraying the surgeons and patient layout, and all of the relative positions of the patient tracker, tracked surgical drill, optical cameras, and user interface.

2.1 Surgical Context and Process

This section will describe the context of the conventional total shoulder arthroplasty, beginning with the patient setup, and later the system setup and protocol.

2.1.1 Patient Positioning During Shoulder Arthroplasty

Commonly, the patient position during a shoulder arthroplasty is in a (lazy) beach-chair position (Figure 2.2). In this position, the patient is initially placed supine on the operating table and moved towards the table edge of the operating side in order to have free mobility of the shoulder/arm that will be receiving treatment. With the use of a foldable operating table, the upper body is positioned at an upward angle from the horizontal, between 30 and 40 degrees (Nashikkar 2019). Holsters, arm holders (opposite arm) and a head holder are then used to secure the body to the table. Furthermore, the lower section of the table which supports the legs is adjusted in order to provide comfort and safety for the patient while in this position. Padding is used to avoid any concentrated contact pressure points. The arm to be operated on remains free and mobile, and will be prepped and draped to be sterile.

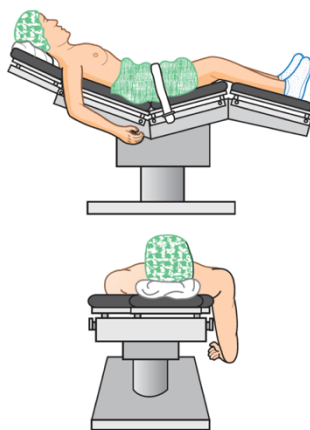


Figure 2.2: In the lazy beach chair position, the patient is laid on the operating table with the thorax angled between 30-40 degrees from the horizontal. The shoulder is situated at the edge of the operating table, with the arm being left free to move. (Adapted from Matsen FA III, Lippitt SB. Shoulder Surgery: Principles and Procedures. Philadelphia: Saunders; 2004:514.)

2.1.2 Conventional TSA Technique

This procedure commonly begins with what is known as the deltopectoral approach, which has been found to be an effective method used to access the glenohumeral joint (Sager 2018). Here, an incision is made through the skin, followed by a separation of the underlying soft tissues (fat, fascia, blood vessels, tendons, and muscles) to reveal the shoulder joint (Chandler 2011). A prying tool is used to expose the humeral head, and guides are then employed to saw off the humeral head, while reamers are used to open a cavity in the humerus (Chandler 2011). These steps are conducted in preparation for the humeral component implantation. Once finished, a temporary component is placed into the prepared vault and a cap is placed over the cut humeral-neck junction to avoid damage to the humerus during glenoid preparation.

Moving to the scapula, retractors are placed around the glenoid, pulling the soft-tissues away and the humeral head posteriorly for optimal exposure (Szerlip 2012). With this added working space, the labrum (cartilage attached around the periphery of the glenoid rim), should be removed (Szerlip 2012). After estimating the position of the glenoid center, a pilot hole is drilled in the glenoid, ideally in the center, normal to the surface, avoiding any significant angling which may cause protrusion through a second cortex. Such protrusions may create issues with cementing material escaping out the back, causing damage to nerves and blood vessels. Despite the potential issues, this pilot hole is mandatory because it acts as a guide for a reamer, which removes the remaining glenoid surfaces (cartilage, cortex and any defects), leaving behind a newly rounded surface in preparation for receiving the implant (Cvetanovich 2020). A mechanical guide is then inserted into this central hole, enabling the surgeon to drill additional holes for glenoid fixation. Since all steps between using the drill guides and the polyethylene glenoid implantation are dependent on the pilot hole, a more accurate placement of this initial central hole is desired. Once

the glenoid vault is prepared, the polyethylene implant component is fixed into position using bone cement (Huri 2020). Hereafter, the glenoid retractors are removed and the humeral head is once again exposed. Upon removal of the humeral cap, trial components are inserted and the humerus is relocated into its proper position of the shoulder joint. The shoulder is then analyzed for component placement, soft-tissue tension, and shoulder joint motion. If the surgeon is satisfied, the trial component is removed and the implantable humeral component is inserted in the humerus. The subscapularis tendon is reattached to its insertion site, and the motion of the joint is tested once more. Closure of the soft-tissue layers as well as the skin then takes place to conclude the surgery.

2.2 Patient Tracker (PT)

As discussed in chapter 1, rigidly mounting a marker array to the bone of interest allows the location of the bone to be tracked. For the patient tracker array, we opted to use an unaltered version of Navigate Surgical's patient trackers, which come in mirrored forms (A and B), designed to be used in different quadrants of the mouth (Figure 2.3). Due to the mirrored design of the A and B trackers, we are able to use these trackers with either left or right shoulder surgeries.



Figure 2.3: Navigate Surgical Technologies Inc. patient trackers A (right) and B (left).

These patient trackers are rigid elements machined from a single piece of aluminum and the tracked pattern is located close to the post that connects to the datum element that attaches to the bone (see Figures 2.3 and 2.4). This eliminates any significant flexion between the marker array and the bone attachment (in contrast to the extended connector used in the Exactech system, which is more prone to being deflected). These laser-engraved patient trackers have a smaller form factor relative to conventional navigation trackers, (Figure 2.2). Finally, in contrast to having all the tracked elements arranged in a plane, as the LED emitters are in the Exactech system illustrated, the optically tracked patterns on our PT are curved around the cylinder, which enables the cameras to view the tracker from a larger range of angles than the planar trackers. Hence, using the NST patient trackers should provide three significant benefits compared to conventional marker arrays.

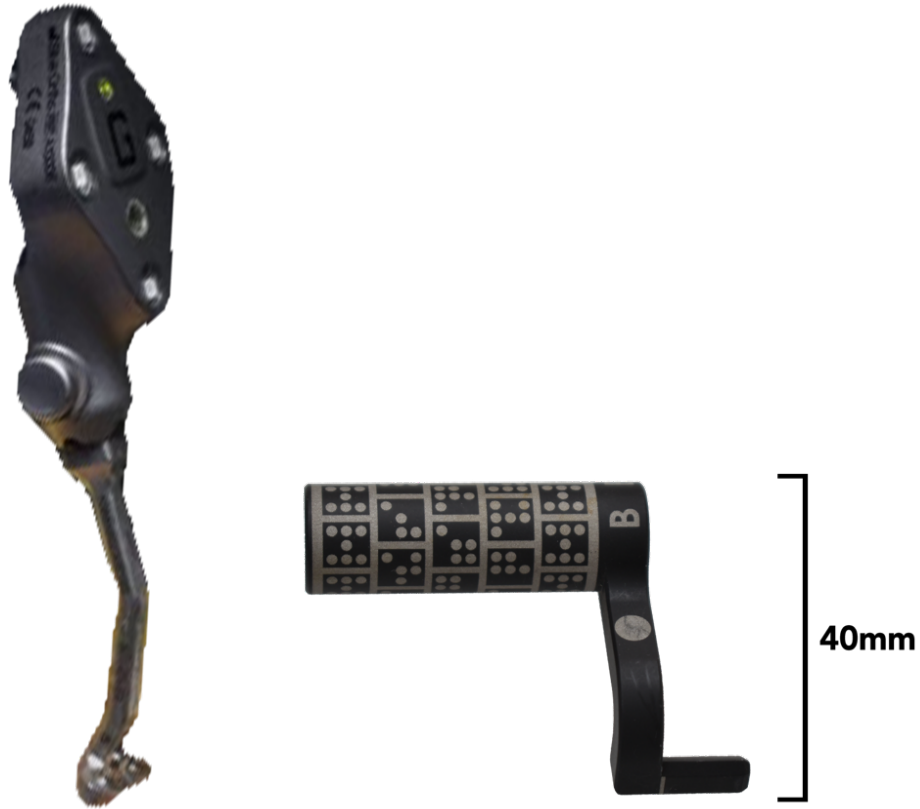


Figure 2.4: ExactechGPS shoulder Anatomy Tracker (left) compared with our proposed tracker (right). Note that the Exactech tracker is approximately twice as tall as ours.

2.3 Fabricated PT- Bone mount

The patient trackers described in section 2.2 were originally designed for dental anatomy, and therefore were not specifically designed to be mounted onto a scapula. In order to make them compatible with our surgery, a custom mount was designed to act as an intermediary between the patient tracker and bone (PT-Bone Mount). The requirements of such a device are:

- i. It must be easily mounted by the surgeon with a single screw.
- ii. It must hold the patient tracker rigidly throughout the surgery.
- iii. It must be attached rigidly to the bone to prevent moving or sliding.

To design this component, we first had to determine what the size and shape limitations are. To understand these limitations, we consulted with an orthopaedic surgeon (Dr. William Regan). We first considered the potential mounting locations on the bone. The primary restriction presented at this step was the relatively small amount of bone surface which is exposed during the surgery. After analysis of the bone exposure during a conventional TSA protocol, it was decided that the most practical location for attaching this mount is on the coracoid process (Figure 2.5).



Figure 2.5: Scapula view from two angles rotated 90 degrees relative to one another (left) with a reference to the coracoid process. Intraoperative coracoid process exposure (right) depicts that this bony landmark is the most prominent landmark available. The right most image matches the orientation of the leftmost image.

A major reason for this decision is that the coracoid process is the only prominent landmark exposed during the surgery, which is not being operated on. In addition, the ExactechGPS Shoulder system uses the same mounting location, so our decision is congruent with their choice of placement (Figure 2.5). Having arrived at consensus on the mounting location, we were able to determine the approximate dimensions available for our mounting device.

We then fabricated an initial prototype that addressed all of the requirements (see Figure 2.6).

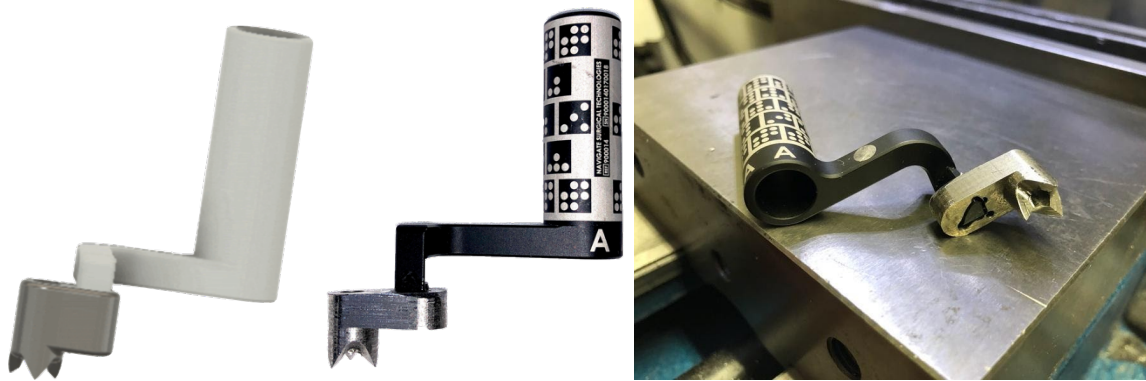


Figure 2.6: Initial prototype of PT-Bone mount with NST tracker attached. CAD design (left), fabricated mount (middle and right).

This first design enabled us to physically mount our patient tracker onto our bone model and inspect for any alterations that might be required. We identified several issues, and made the following changes in the second prototype iteration:

- i. We changed the angle of the patient tracker orientation on the mount, such that it would be more clinically reasonable. This was done by positioning the axis of the marker array at a 45-degree angle exposing the face of the marker array to the cameras (as seen in Figure 2.7).

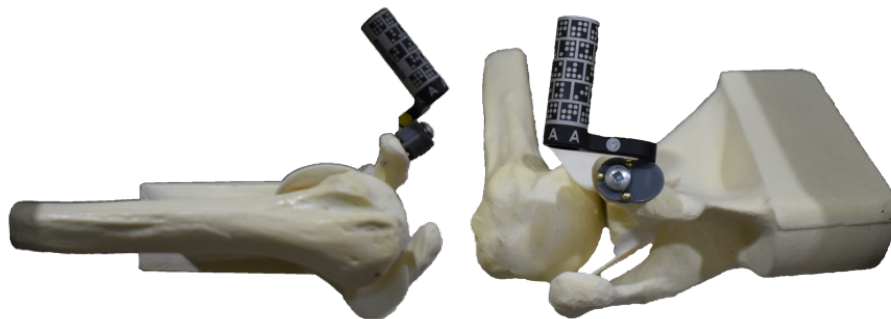


Figure 2.7: Patient tracker rigidly attached onto the coracoid process of the scapula by means of our custom designed PT-Bone Mount. The tracker is positioned similarly to how it would be used in surgery. A side view of the setup (left) shows the apparatus mounted onto a left shoulder. The image on the right shows the camera perspective of the patient tracker when the cameras are located near the head of the patient.

- ii. We increased the distance between the feet in order to provide a more stable base.

- iii. We replaced the original pyramidal spike design with pins that have shoulders, which enabled the feet to penetrate into the bone to a known and controllable depth, preventing unwanted translation and rotation relative to the coracoid.
- iv. We also changed the feet from 4 feet to 3 feet. Having three contact points prevents any rocking of the PT-Bone mount, as predicted by minimum constraint design heuristics.
- v. We designed a side-oriented channel to accept the marker posts from either direction. This enables us to use a single PT-Bone Mount for both A and B trackers, which would allow this device to be used in both left and right shoulder surgeries.

To build this final PT-Bone mount, we used a Formlabs Form 2 SLA 3D printer to print using their Grey Pro Resin, and added holes in the 3D printed mount for metal pins to be inserted into (Figure 2.8).



Figure 2.8: Computer rendering of the final prototype of the PT-Bone Mount illustrating both top and bottom surfaces. This mount will accommodate PT A for left shoulder surgeries and PT B for right shoulder surgeries.

2.4 Surgical Drill Tracking

To track the surgical drill using the Navigate Surgical Technologies tracking system, we needed to design an appropriate marker array, attach it to the surgical drill and calibrate it. At that point, the system can track the drill's position in 3D space.

2.4.1 Surgical Drill

We chose to use the CONMED HALL 50 surgical drill (see Figure 2.9) as it is similar to the drill normally used in this procedure, and it was easily accessible to us. To track this drill, we generated a custom marker array which we decided would be situated on the barrel, where it would be most visible to the cameras during surgery. To create this array, we required the engineering drawings for the drill. Since we did not have access to these files, we generated our own by measuring all critical surfaces relating to the barrel of the drill. We conducted these measurements using calipers in order to extract the key relationships that we needed in our model, and came up with a simplified 3D CAD design (Figure 2.9). This virtual model was also required by the NST User Interface (UI). To upload this design to the UI, we needed to convert our solid body (.STEP) file into an OBJ Blob. This step was completed in Autodesk Fusion 360. Using this same software, the drill origin for the model was then realigned such that it was situated where the origin of the marker array was defined. The x, y and z axes in the solid model were also aligned to be congruent with the axes of the marker array. This aligned OBJ Blob served as a visual representation for the live 3D view during surgery, as well as for the manual registration process which will be discussed later.



Figure 2.9: CONMED HALL 50 surgical drill (left), along with the 3D CAD model derived from measurements made on the drill (right).

2.4.2 Marker Array

With the CAD design completed, we moved on to generate a custom marker array for this drill using proprietary software developed by Navigate Surgical Technologies (NST). Creating tracked patterns to be engraved on the drill is a multi-step process. First, predefined dice-shaped markers are aligned on a planar surface and arranged with equal distances between the centers of each marker (Figure 2.10). These dice-shaped markers are a standard used by NST. This planar 2D marker array is then placed over the drill, and the desired placement is found by aligning the central dot (known as the local origin) with the central drilling axis of the drill.

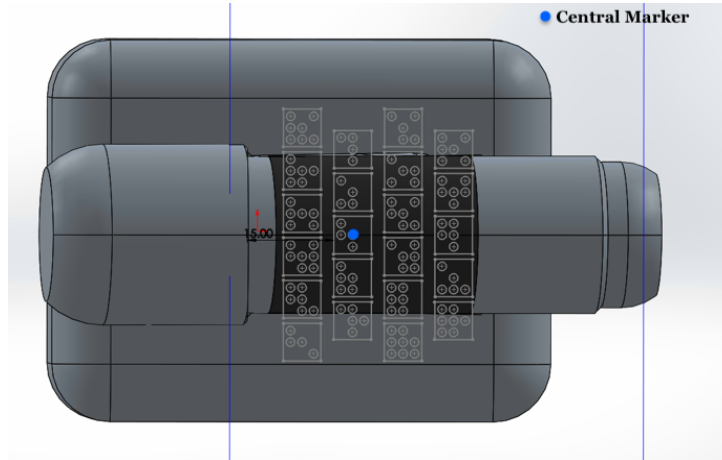


Figure 2.10: 2D marker array overlaid onto the barrel of the surgical drill.

Lastly, we wrapped the marker array around the diameter of the drill barrel. To map this 2D plane onto the curved surface of the cylinder, we used a cross section of the surgical drill barrel aligned perpendicular to the drill axis to determine the translation for each of the dots on the marker (Figure 2.11) The marker array is placed tangent to the top of the cylinder, and we know that the distance of our dot from the local marker array origin will become the arc length once wrapped. Given the radius of the cylinder, we find the angle φ using $\varphi=s/\rho$, where s is the arclength, ρ is the radius, and φ is the angle in radians. Now that we know φ , we can calculate the x and y coordinates of the translated dots relative to the central axis of the drill barrel. We do this using $x=\rho\cos\varphi$ and $y=\rho\sin\varphi$.

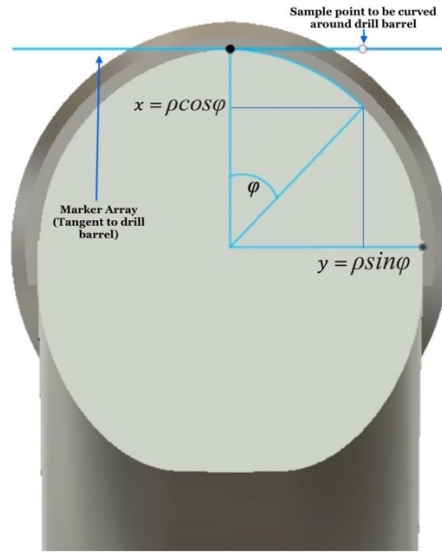


Figure 2.11: Cross section of drill barrel. Mathematical computations for translating the 2D planar marker array into the 3D cylindrical coordinate system.

Once the computations of the marker array have been completed to wrap the dots around the cylinder, we get a configuration file specific to the drill, which specifies the expected location of each dot around the drill barrel (Figure 2.12).

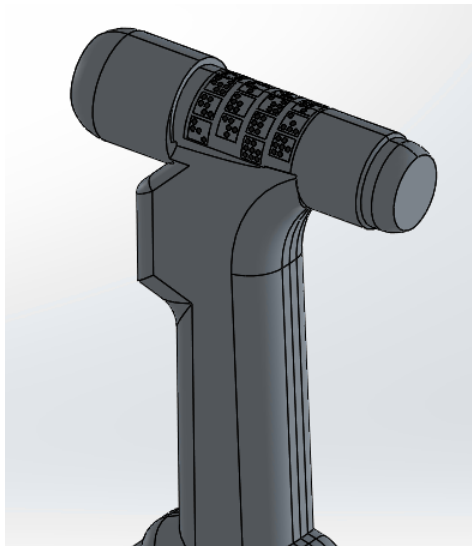


Figure 2.12: Marker array wrapped around drill barrel.

2.4.3 Marking the Drill

Ideally, we would laser engrave the tracked marker array directly onto the drill, as NST normally does with their dental handpieces (Figure 2.13).

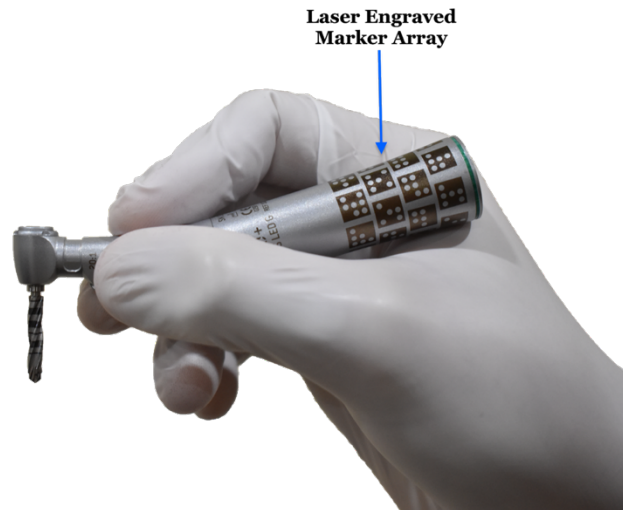


Figure 2.13: NST surgical handpiece with laser engraved marker array.

The locations of the dots on the laser engraved marking would then be measured with optical metrology equipment, and a drill specific configuration file would be produced, acting as a registration between the markers and the tool. However, due to time and equipment availability constraints, we opted to use a white sticker with the pattern printed on it instead (Figure 2.14). These stickers were printed on 300-micron thick paper using a “Dymo Label Maker 450 Printer”. The pattern was then cut out of the larger sticker stock and placed on the barrel of the surgical drill (Figure 2.14). This method worked sufficiently well for our system verification purposes, so we used the sticker throughout the experiments reported here.



Figure 2.14: Marker array printed on sticker (left) and later attached to the barrel surface of the drill (right).

2.5 Drill Length Measurement

When mounting the drill bit into the chuck, there is variability associated with the mounting. Hence, after we mount the drill bit we have to perform a calibration process. Our proposed calibration process is to use a feature built in to the NST UI, which prompts the user to touch the tip of the drill to the dot on the patient tracker (Figure 2.15). As long as the drill is substantially perpendicular to the face of the dot, the computer will sample the drill length nine times per second, following which, the system automatically calculates an average of the measurements made while in contact with the point and returns an estimate of the position of the tip of the drill relative to the marker array.



Figure 2.15: Laser engraved dot on NST patient tracker, used to calibrate the drill length offset.

2.6 Stereo Cameras

For the tracking cameras, we used an unaltered version of the NST stereo cameras. These are a pair of Point Grey FL3-U3-32S2M-CS cameras separated by 222mm and angled at 18 degrees from one another (Figure 2.16). This angle isn't crucial for our present purposes, but for the ultimate clinical application the cameras' fields of view should overlap at the designed target distance from the camera pair to the surgical site in order to provide the largest combined field of view (x/y) possible at that design distance. It is, however, important that the angle between the cameras does not change once they are calibrated, as this will lead to inaccurate tracking. The NST camera mount is designed with a rigid aluminum body to minimize deviations arising from both thermal and mechanical influences (Figure 2.16). As their unmodified setup is currently designed, the ideal working range is around 710 mm. The accuracy drops off if the cameras get too close or too far from the targets, and the chosen lenses are selected to provide a working focal range of approximately +/-10cm around that point. Since our verification testing was conducted in a controllable environment in which the distance between the cameras and the patient tracker was not altered, this setup worked acceptably for our experiments.



Figure 2.16: Point Grey FL3-U3-32S2M-CS cameras mounted onto the NST stereo camera mount made of a rigid aluminum construction, acting as both a heat sink and mechanical mount.

2.7 Binary CT scan

The Navigate Surgical software requires a DICOM file of the object to be operated on. In a clinical workflow, this would be acquired in the form of a CT scan of the patient’s shoulder, but for our preliminary validation, we simply needed a DICOM-formatted 3D model of the specimen that we are going to work with. Hence, we purchased a phantom model from SAWBONES (USA). They did not make a DICOM file available, but could provide an STL file instead. We therefore opted to generate our own binary DICOM model using the STL mesh body file that we purchased from SAWBONES. To begin, we had to determine the reference frame conventions used by the NST software. We found that the user interface (UI) presumes that the DICOM origin is at the center of the model’s bounding box in all three axes. Hence, we set the origin of the mesh body to be in the same location prior to the conversion. To reorient the origin, we used the software “Autodesk Fusion 360”, which has a built-in function to do so, and then exported the .STL file with the fixed origin. We then converted this .STL file into a binary DICOM file using the software, Slicer 3D, and the results are shown in Figure 2.17.

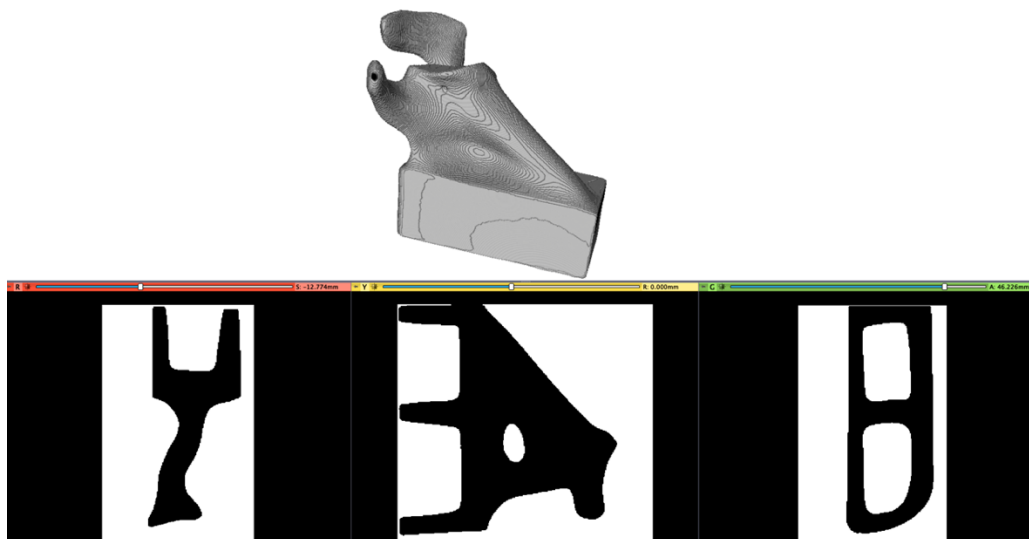


Figure 2.17: Binary simulated CT scan (below) generated from a .STL mesh body file (above) using Slicer 3D.

2.8 Glenoid Implant

While our study did not require a physical model of the implant, since we limited ourselves to implementing the drilling guidance and execution step that occurs prior to implant placement, we did need a virtual model for use in the surgery planning phase. To acquire such a model, we purchased a glenoid implant from SAWBONES (SKU:1718), and performed a CT scan of the model using an XtremeCT HR-pQCT scanner (Scanco Medical) located at the Centre for Hip Health and Mobility. The resulting DICOM file was then used to generate a 3D mesh body, which was imported into the NST user interface.

To perform the conversion step between DICOM to an .OBJ blob, which is the file format required by the NST database, we began with a custom python script developed by the R&D team at NST. This script takes a DICOM file as an input, as well as attributes for the Hounsfield levels (HU) desired, and outputs an .OBJ blob (Figure 2.18).

This .OBJ file of the glenoid was then aligned using a CAD software package (Fusion 360) such that the origin is placed at the centroid of the central peg, where it comes into contact with the rest of the glenoid body (Figure 2.18). When the glenoid implant is pushed all the way into the prepared glenoid vault, this origin point will be at the surface of the anatomic glenoid. Hence, the Z axis for the implant model, which is aligned with the central axis of the central peg, was used as our target trajectory axis. Once this aligned .OBJ blob was created, it was imported into the NST database, where it was treated by the software as a dental crown (the standard implant model used in the dental navigation software). To perform this task, the blob file was uploaded to replace a pre-existing blob representing a dental crown. After loading the blob, the glenoid model was available for selection in the NST software and would appear on the planning and execution screens in the desired shape.

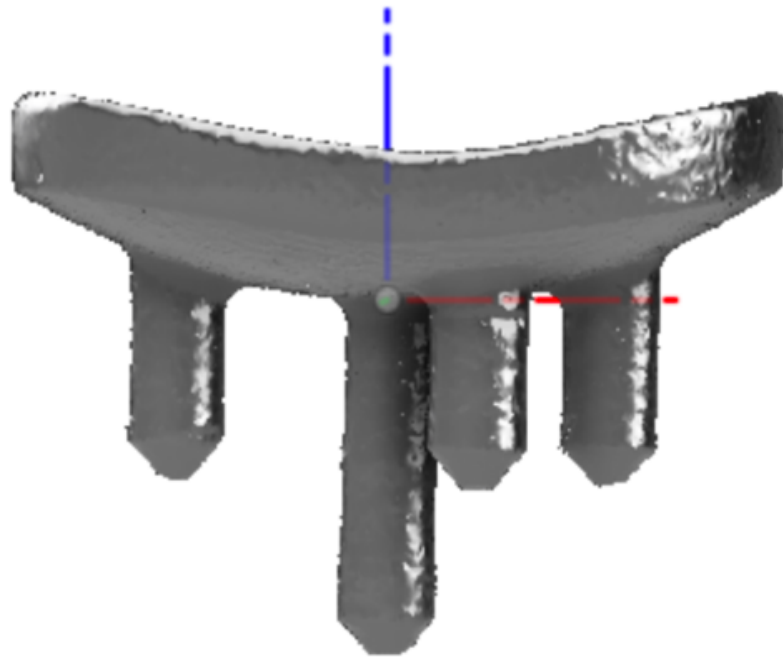


Figure 2.18: Resulting .OBJ mesh body for the glenoid implant generated from a DICOM file from a CT scan. The origin is centered on the top of the central implant peg with the Z axis aligned with the axis of the central peg.

2.9 NST User Interface 2.6 Planning, Registration, and Guidance Modules

We used an unmodified version of the Navigate Surgical user interface, which walks the clinician through several preparation steps. Prior to start-up, the user first imports the anatomical model into the system database. Upon launching the program, the user must pick the imported model and create a new case. The system will automatically produce a 3D mesh body and display it during subsequent steps. This 3D surface body is used as a virtual model of the patient's anatomy during the case. Furthermore, it is used for the registration of the tracked bone, as well as for the surgery planning module.

2.9.1 Planning Module

In the planning workflow for dental procedures, the surgeon would usually align a dental implant post onto the surgical scene, and the UI will enable them to demonstrate a dental crown simply for visual aid. Unlike the dental procedure where there are two separate concepts of implant and crown, in TSA we only have a single component, the glenoid implant, and these two things are a part of the same object (Figure 2.19).

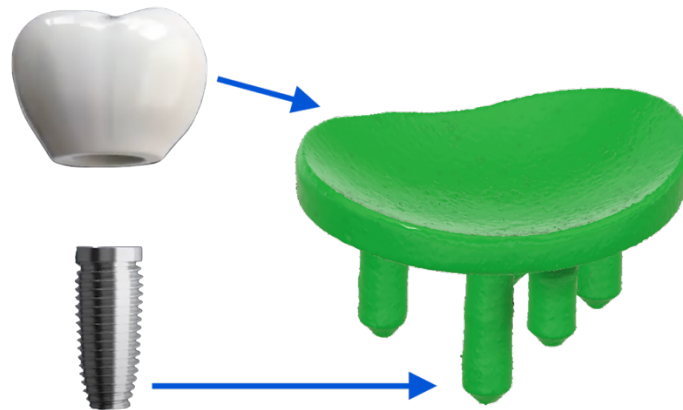


Figure 2.19: Resulting single piece glenoid implant component (green) which incorporates both the dental implant (grey) and dental crown (white).

Hence, we have repurposed the dental surgery code for this as there are a couple of concepts that we need to accommodate. These kludges are things that we wouldn't do in a subsequent system, but we are doing them now to make the system work for our shoulder application.

Once we import the glenoid component (described in section 2.8) into the scene, we can manipulate the position of it using the built-in functions to rotate and translate it to the desired surgical position (Figure 2.20).

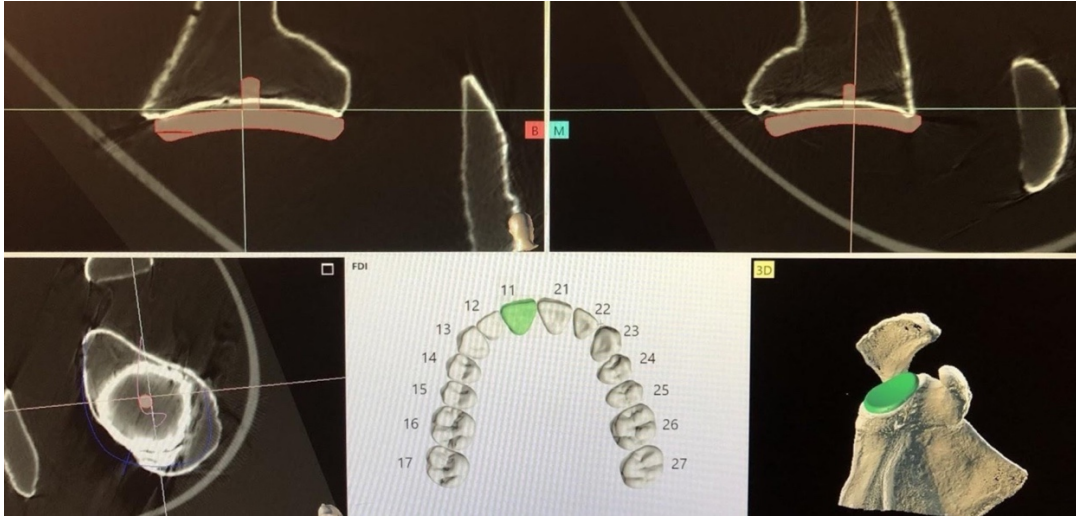


Figure 2.20: Glenoid component imported into the user interface is shown during the planning phase, and is manually manipulated relative to the CT scan of the scapula model.

We manually aligned the version and inclination relative to the scapula. Since the actual surgery trajectory is determined by the dental implant and not our glenoid component, we need to align the dental implant to the central peg of the glenoid component in order for our drilling trajectory to be generated along the axis of this central peg. To perform this transformation, we find the 4x4 transform matrix (T_{IC}) in the NST database which was created to define the position of our glenoid component relative to the CT scan (Appendix B, Equation 4.4). We then simply copy this transform matrix and paste it into the 4x4 transform matrix that defines the positional offset of the dental implant relative to the CT scan. Now this dental implant is perfectly aligned with the central peg of our glenoid component. We can successfully do this since we had properly aligned the origin of our glenoid component in section 2.8.

2.9.2 Registration Module

In the registration module, the goal is to register the patient tracker to the patient's scapula. In a real surgery, this step is a critical contributor to the overall procedure accuracy, but in our

experiments, we only require a nominal registration as we are initially focusing on evaluating the accuracy and repeatability in targeting and execution, rather than on registration, as registration in and for a surgical context requires more complete consideration of the anatomical situation (e.g., surgical exposure, presence of osteophytes, periosteum, and cartilage, etc.) than we had capacity to address within the time limitations of this thesis (especially given the impact of COVID restrictions on research throughout 2020).

This nominal registration process involved two main steps:

1. Calibrating the drill tip to allow the drill to be used as a pointing tool
2. Performing a 3-point manual registration

To calibrate the drill tip, which is also normally done in the standard NST workflow, the system prompts the user to touch the drill tip to a drill length measuring dot on the patient tracker (Figure 2.15). This allows the system to calculate the position of the drill tip along the axis defined by the printed marker array on the drill.

After completing this step, the user is asked to sequentially touch the tip of the drill to three points on the bone model which the patient tracker is attached to. These points correspond to three pre-selected points on the CT scan. Doing this effectively enabled us to define a reference frame based on the anatomical points as seen in Figure 2.21, in which we were able to create a transform (T_{TGa}) that defines the displacement between the tracker reference frame (T) and the anatomic glenoid frame (G_a). Similarly, in the CT scan this effectively defined a coordinate frame based on the three selected points, which produces a transform from the bone reference frame (B) to the virtual CT glenoid frame (G_c). Solving the three-point correspondence problem, which happens automatically by the NST software, brings these two frames (G_a and G_c) into agreement with each other. Hence, the transform from $B \rightarrow T$ is $B \rightarrow G_c = G_a \rightarrow T$. In other words, by performing this

registration our system can assume the location of the drill tip relative to the bone, and any error between matching G_a and G_c is the registration error.

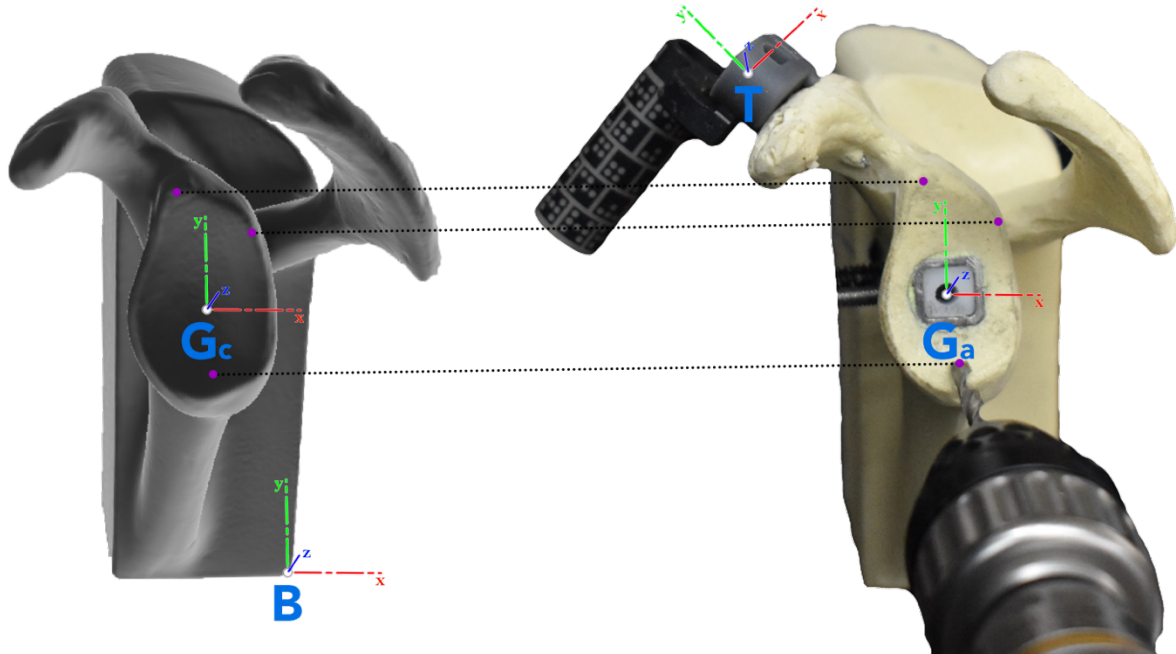


Figure 2.21: Reference frames associated with registration of the patient tracker (T) to the bone model (B), by probing three points (purple) on the native glenoid (right), and selecting the same three points in the virtual model (left).

Since the NST system was designed for dental use, it normally only allows for points to be selected near to the “jaw curve” which is drawn during the planning phase. This is a built-in safety feature in the NST UI to prevent dentists from registering their drills outside of the anticipated area. To work around this safety feature, which is unneeded in TSA, a “jaw curve” was drawn around the glenoid rim in the planning phase. This limited us to selecting points only near the glenoid rim, which is likely suboptimal in real surgeries, but this limitation was acceptable for our purposes as we required only a nominal registration.

2.9.3 Guidance Module

At the “Perform Surgery” screen, the user is prompted with four sub views which show three orthogonal views and a 3D perspective view of the surgical scene. The 3D view only becomes active once both the drill and patient tracker markers are both in view of the camera. Otherwise, a live view of what the cameras see is presented. If the system detects a pattern of dots which matches the expected layout for both the drill and the patient tracker, as per the specific uploaded configuration file, the 3D view will become visible, and the user is able to proceed Figure 2.22.

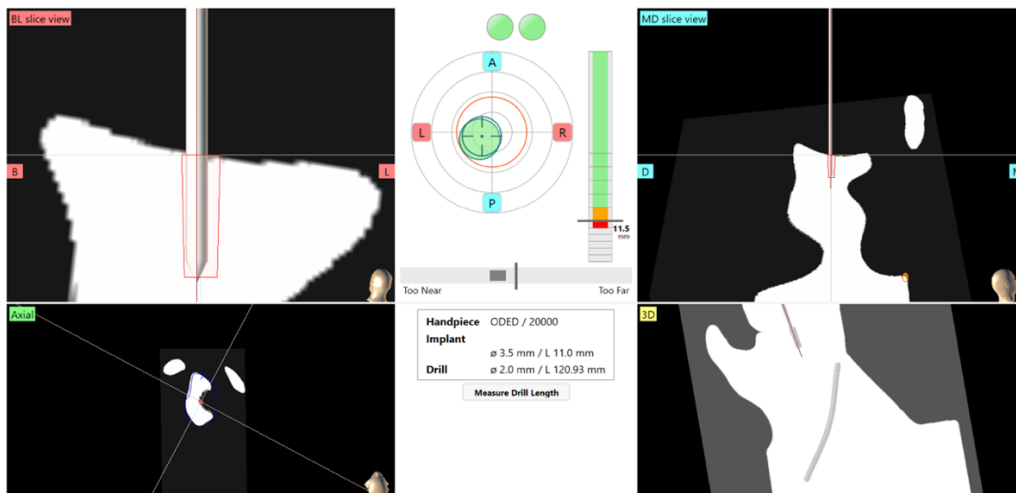


Figure 2.22: NST UI representing three orthogonal views (top-left, top-right, bottom-left) and the 3D view (bottom right) when both trackers are in view of the cameras.

Chapter 3: Methods – Evaluation Process

In the previous chapter, we discussed the design and implementation of a less-obtrusive tracking system for Total Shoulder Arthroplasty. In this chapter, we present the methods used to verify the feasibility of the proposed system, as well as its tracking and targeting accuracy and repeatability. We first present the design of a custom drilling jig that can accommodate plastic inserts to serve as drilling targets. We then present tools and a protocol for accurately measuring the achieved trajectories of the drilled trials. Lastly, we describe how we process the resulting data and compare our trials to the planned trajectory in order to determine our system accuracy and repeatability.

3.1 The Concept

To verify our system, we wanted to develop a jig which would allow for an anatomically-realistic drilling experience when performing the navigated mock surgery while still allowing us to accurately measure the resulting drilled trajectories. One way to perform these trials would be to purchase 90 separate scapula models, one for each trial, and then measure the drilled hole locations in a standardized manner for all models (assuming all models are manufactured sufficiently identically). However, purchasing so many models would not be economical. To eliminate this concern, we decided to use a design which would accept replaceable plastic inserts for each new trial. This design would not require the use of fluoroscopy, and would work with a single bone model for all 90 trials. At the end of each trial, the plastic insert with its drilled hole would be replaced with the subsequent plastic insert. The axis of the drilled trajectory for each plastic insert was then measured in a standardized manner, and the resulting clinically-relevant measures related to inclination and version angles were computed. Developing such a jig enabled

us to evaluate the precision of our technique by effectively emulating the same kinds of tests that were conducted for the ExactechGPS® Total Shoulder 510k summary report in their FDA submission, which served as the basis for their regulatory approval. These include the verification that the hardware all functions as intended with the modified software, as well as a comparison between the system results and the pre-plan.

3.1.1 Drilling Jig Setup

We acquired a scapula model from SAWBONES (SKU: 1050) which was equipped with a feature that allowed it to be held with a vise (see Figure 3.1), and used a CNC machine to drill a 15.4mm hole nominally centred on the desired entry hole and oriented with the target trajectory. Without changing the setup, we removed the drill bit and inserted into the chuck a 316 stainless steel square tube. We used a square tube to ensure repeatable rotational positioning of the plastic inserts, and a screw in the metal tube to ensure repeatable axial positioning. This tube had 12.7mm outer side lengths, and 9.525 mm inner side lengths. We then used the CNC machine to push this tube straight down along the same trajectory used to drill the round hole in the polyurethane bone model.



Figure 3.1: SAWBONES scapula bone model in the midst of preparation to be used as our surgical jig.

The pointed edges of the square stainless-steel tube were used to effectively broach the sides of the round hole, creating a perfect fit for the square rod. The stainless-steel tube was then anchored even more securely onto the bone model by pouring cyanoacrylate (‘Superglue’) down the cavities on the outside of the steel tube. A screw was then inserted into a hole drilled through the steel tube such that the outer edge of its threads was nominally 22mm from the top of the square pipe. This was used as a stop limit for the plastic inserts. Lastly, the base of the bone model was glued onto a low carbon steel plate for easy vise mounting without damaging the model itself (Figure 3.2).



Figure 3.2: Prepared bone model mounted onto a steel block. The steel tube insert is visible in the glenoid fossa at top.

3.1.2 Plastic Inserts

To create the plastic inserts, which would be the material used for drilling into, we began by purchasing slightly oversized square Delrin acetal resin rods of size 10mm x10mm (length: 30 cm). Delrin was used as it machines easily and was readily accessible. Using a CNC mill, we machined down each rod to provide a sliding clearance fit to the inner dimensions of the stainless-steel square tube, which allowed the plastic to slide in snugly. One side of each long rod was then marked with a permanent marker prior to cutting, which enabled us to identify the orientation of the inserts when they were reinserted. Finally, these rods were manually cut down to 22 mm length pieces on a band saw, and the 8 edges of the cut surfaces were filed down to remove any loose-hanging material (Figure 3.3). While these Delrin blocks had uniform density unlike the bone that

will be drilled during a surgery, it should have no effect on the initial alignment of the surgical drill.



Figure 3.3: 22mm length prepared Delrin specimen, marked with blue marker for proper orientation.

3.2 Measuring pins

To conduct the measurements of the post-operative drilling trajectory, custom-made measuring pins were machined on a lathe (Figure 3.4). The manufacturing process began with 6.35mm diameter 18-8 Stainless Steel Unthreaded Spacers, which were purchased online from McMaster.com (PN 92320A097, and 92320A309) in lengths of 25.4mm and 50.8mm. Half of the length of each pin was then machined down to a diameter of $4.4\text{mm} \pm 0.1\text{mm}$, which would fit snugly into the drilled holes inside the Delrin plastic trials (Figure 3.4). 4.4mm is the same diameter as the drill bit used for the surgery, which is also the same as the central peg of the glenoid implant we acquired from SAWBONES.



Figure 3.4: Custom made measuring pins with a stem machined to $4.4\text{mm} \pm 0.1\text{mm}$.

3.3 System Setup on Trial Day

Three participants each conducted thirty trials of mock surgery. The choice of thirty repetitions was made to strike a balance between the desire to have as many trials as possible to obtain a good estimate of the precision, and the desire to not overly impose on the time required of the participants (approximately 1 hour for the thirty trials). We chose three participants with differing levels of experience and expertise to check for potential differences in performance related to overall surgical skill level: an attending orthopaedic surgeon with significant experience in TSA, an orthopaedic fellow gaining experience in TSA, and the navigation system developer (an engineering student). The participants conducted their trials in this respective order, and all were provided the same target. The stereo cameras were mounted on the back of a computer monitor, which was used as the targeting display (Figure 3.5). The prepared bone model jig (described in Section 3.1.1), was mounted vertically on a vise that was rigidly clamped to a table. Registration (as described in section 2.9) was performed once and used for all trials by all participants to ensure that the registration localization error, which is the error in locating the actual points, was the same for all three participants. The surgical drill (as described in section 2.4) was

provided for the user, and the drilling was conducted for each of the thirty trials. After a new Delrin specimen was inserted to the stainless-steel tube, it was locked into place using a long-threaded screw that was finger-tightened. As described earlier, an additional screw was already in place crosswise between the two walls of the stainless-steel tube at a nominal depth of 22mm in order to act as a repeatable axial locator for the plastic inserts.



Figure 3.5: Surgical system setup on day of the mock trials, with the attending orthopaedic surgeon holding the drill. The cameras were mounted on the back of the monitor mount, looking down at the surgical drill and patient tracker. The drilling jig was mounted vertically on a vise which was clamped down to the table.

At the beginning of each trial, a thin layer of plasticine was spread over the glenoid surface to prevent the user from making use of visual cues in placing the drill on the surgical surface (Figure 3.6). This effectively forced the user to rely strictly on the navigation user interface. Once each trial was completed, the tightening screw was loosened, the long measuring pin was inserted into the drilled hole and used to pluck the plastic out of the square stainless tube before the next plastic specimen was inserted.



Figure 3.6: The uncovered drilling jig (left) and the glenoid surface covered with plasticine (right) in order to prevent the user from using visual cues related to the plastic insert and tube when choosing the drill entry point.

3.3.1 Mock Surgery Instructions

The participants were asked to conduct their thirty trials at their own pace and with no explicit time limitations. They were allowed to stop drilling mid surgery to readjust their drill angle as needed, and continue drilling. They were instructed to drill to a depth between 13-15mm as per the readout on the NST UI. At the end of each trial, participants were asked to stop the drill rotation prior to retracting the drill to prevent any added material removal during the retraction.

3.4 Trial Measurements

Once all 90 trials were completed, the drilling axes for all trials were measured and compared to the pre-planned trajectory. To begin the measuring process, the drilling jig was mounted on a CNC machine (Figure 3.8) oriented such that the glenoid fossa was substantially horizontal, and the measuring pin substantially vertical. The tool attached to the CNC machine was a manual 3 axis probe (Haimer 80.365.30.FHN Universal FH 3D Sensor), which effectively enabled the machine to act as a coordinate measuring machine (CMM). An arbitrary point on the bottom left corner of the jig was chosen and set as the zero point, such that all points on the bone

which were probed resulted in positive values for all three axes (X,Y,Z). Seven points were then probed directly on the bone model (Figure 3.7), which were later used to conduct an iterative closest point (ICP) registration (described in section 3.6 below) that enabled us to map the measured points into the model's reference frame for comparison against the planned trajectory.

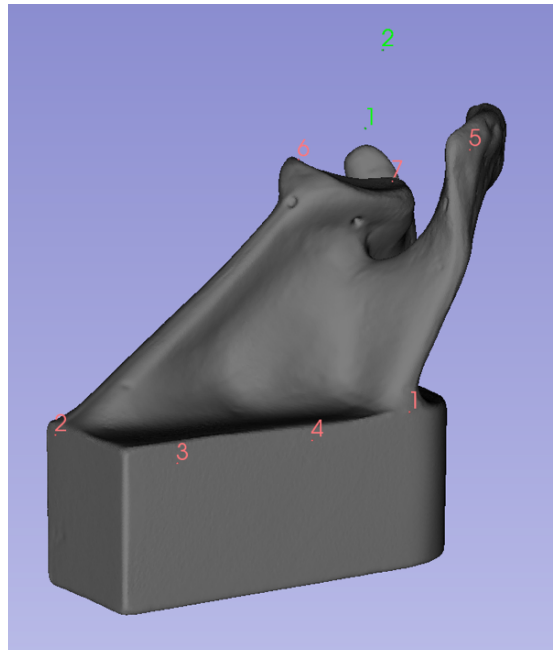


Figure 3.7: The seven points indicated in red were the points probed on the bone model to later be used with the ICP. These were selected in accordance with minimum constraint theory to provide reliable and repeatable registrations. The green dots represent the points measured for the long and short pins of a specific trial.

Once the registration points were acquired, one of the drilled Delrin blocks was inserted into the stainless-steel tube in the bone model. The alignment was congruent with the positioning used during the drilling trials, with the mark made by the felt pen marker used to orient the sides, and the entrance point of the drilled hole used to determine the ‘up’ orientation. The 4.4mm diameter side of the long pin was inserted into the hole at this point and pushed in snugly to some arbitrary depth. The probe was then manually positioned over the top of the pin, and then brought down until it registered contact with the pin. We then pulled back just a little, until there was no displacement registered on the probe dial, but the tip of the ball was still under the plane of the

hole in the pin. Then we moved it in the x-positive direction until contact was registered, we performed the same for the x-negative, split the difference between the two contact points and brought it to the center. We then performed the same probing for the y-positive and y-negative finding the center of the hole in the pin. At this point we plunged the ball probe straight down just to sit the ball, and preloaded it by 300 microns to ensure that the ball was properly seated on the rim of the hole (Figure 3.8). This was consistent across all measurements.

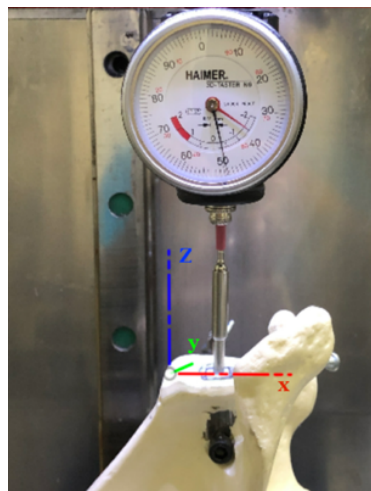


Figure 3.8: The drilling jig was mounted on a CNC machine holding a manual 3 axis probe (Haimer 80.365.30.FHN Universal FH 3D Sensor), and was used to find the center of the holes located at the top of the measurement pins by probing and finding the middle point between the x+ and x- limits, as well as y+ and y-. The ball was then plunged down to ensure proper seating on the rim.

3.5 Drilling and Re-insertion Accuracy Tests

To ensure that there was no significant added error from the probing or reinsertion of the Delrin plastic insert into the drilling jig, two additional tests were conducted.

The first was a **reinsertion test** which considered the mounting repeatability of the plastic inserts. This was done by inserting the long pin snugly into the drilled hole, and then probing to find the location of the top hole of the pin. The plastic piece was then removed with the pin still rigidly attached, and immediately reinserted into the jig. Once again, measurements were taken to find the

top hole, and the plastic piece was unmounted yet again. This was conducted 30 times to yield the variance amongst the trials. This test is indicative of the re-insertion accuracy.

Next, we had to quantify any **variation resulting from the drilling process** itself. To do this we placed our jig under a CNC milling machine, and nominally aligned the drill at the center of the square shaft. We loaded a plastic insert and ran a G-code algorithm to automatically drill down to a specified depth of 15mm. Without moving the jig nor the CNC milling head, we replaced the plastic insert with a fresh piece and ran the code again. Once thirty specimens were drilled, they were also measured on the CMM machine using the long pin. Each specimen was mounted into the jig, and the long pin was inserted into the hole. We probed for the center of the hole, and the X,Y,Z coordinates were noted down.

3.6 Comparing Probed Points to Plan.

In order to compare our probed points to the pre-planned trajectory, we had to consider the reference frames involved with our testing. Figure 3.9 depicts the different reference used to represent the various points of interest, from the probed data (P) to the mesh body (S) to the CT scan (C) and finally the implant reference frame (I). It also identifies the Euclidean rigid-body transformations (T_{xx}) required to map the point locations between the various reference frames.

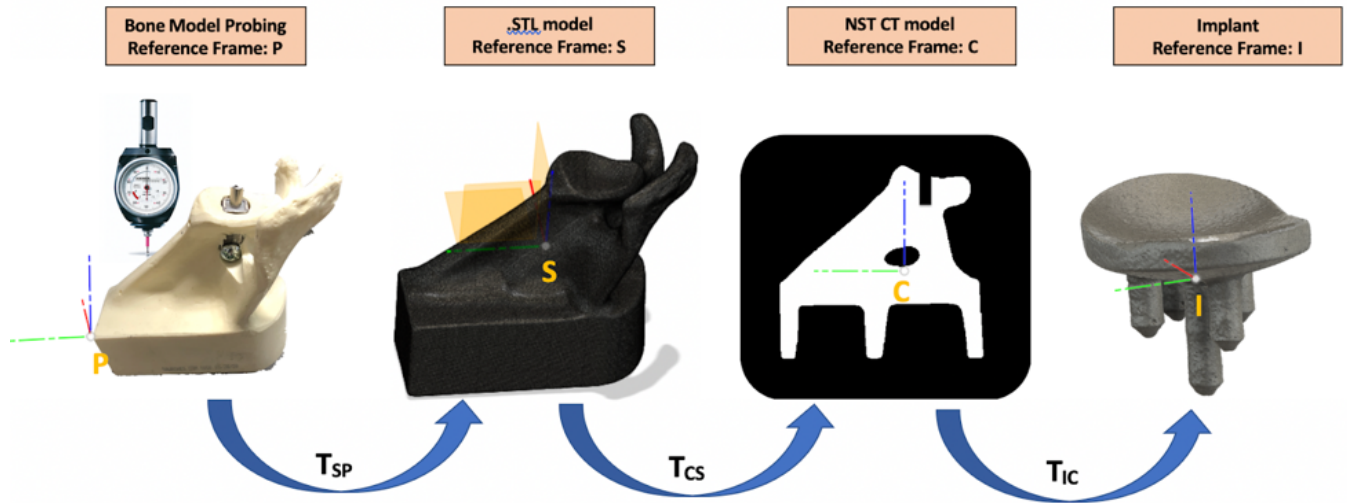


Figure 3.9: Overview of project reference frames P, S, C, and I, as well as the transform matrices derived and utilized (T_{SP} , T_{CS} , T_{IC}).

The probed points on the pins for each trial were nominally aligned with the Z axis of the CMM machine and are initially recorded in the reference frame of our CMM machine (reference frame P). Since we ultimately wish to express the locations of these points in the implant reference frame, I, in order to compare their locations with those of the pre-planned trajectory, we need to determine the various intervening transforms (T_{SP} , T_{CS} , and T_{IC}). In order to determine the 4x4 transform matrix (T_{SP}) which defines the positional offset between our P and S reference frames, we employed an iterative closest point matching algorithm (ICP). This algorithm is frequently used to register two or more 3D point clouds (Yuan 2015). Using the ICP algorithm requires at least one of the point cloud collections to represent a surface mesh; the other collection can be a smaller set of discrete points. Before employing the ICP, we manually aligned the two point-clouds using 3D Slicer to bring them as close as possible, as the ICP algorithm uses a local optimization technique and requires the initial guess to be reasonably close to the true optimum in order to converge correctly. This initial manipulation yielded a new frame, S1, and an associated 4x4 transform matrix (reported by Slicer) which we termed T_{S1P} (Appendix B, Equation 4.1).

With the points now nominally aligned, we ran the ICP algorithm directly in 3D Slicer using the freely-available IGT (Image-Guided Therapy) extension (Ungi, Lasso & Fichtinger, 2016). We conducted the maximum number of iterations (1000) allowed by the user interface, as this added just a few seconds to the computation time and marginally improved the accuracy of the resulting registration. Following registration, the RMS fitting error between the set of seven probed points and the mesh representing the scapular model was 0.007 mm. Note that we have not directly calculated a target registration error, which would measure the deviation between the actual and estimated positions of surgical target points such as the drill hole entry location - the target registration error is likely to be larger than this fitting error value. Once the ICP was conducted, it produced yet another 4x4 transform matrix, T_{s1} , which described the transform between the S1 reference frame and S (Appendix B, Equation 4.2). Multiplying $T_{s1} * T_{s1p}$ yields T_{sp} , the transform matrix which describes the position of the probed points within the S reference frame (Appendix B, Equation 4.3).

Since the S and C frames were designed by construction to have the same origin (as described in section 2.7) the transform between S and C is the identity matrix, so $T_{sp} = T_{cp}$. To confirm that reference frames S and C are indeed the same, I used 3D Slicer to visually represent the points after transformation. The probed points were moved to their expected location about the glenoid surface (with the three points generating a drill line into the glenoid) when transformed to reference frame C. Similarly, the planned implant points were transformed via T_{ic} (produced by

the NST software during the planning process¹), and landed where they were visually expected, with one point at the surface of the glenoid, and the other point 11mm deep below it in the bone. A sample calculation of the transfer of points through the transform matrices has been provided in appendix C. The code used to transform the points through the 4x4 matrices is available in Appendix D.

3.7 Rotating Probed Points to Match the Conventional Axes Layout.

The implant reference frame is oriented such that the positive Y axis is directed in the anatomically superior direction. This is true for the mock trials, and the phantom verification testing consequently (Figure 3.10). However, when we probed the points on the CMM, the vise holding the bone was aligned such that the x+ was in the superior direction of the implant reference frame (Figure 3.10). In order to turn the probed data so that the Y+ is in the superior direction, we simply rotated the probed points counter clockwise 90 degrees after bringing them into the implant reference frame “I”. We did this by making the new x values equivalent to the old y values *-1, and making the new y values equivalent to the old x values. The resulting values enable us to compute Version as angular deviation in the X axis, and inclination as angular deviation along the y axis.

^{1 1} Note: the transform matrix produced by the NST software describes the mapping from the implant (reference frame I) to the CT reference frame (C), or T_{CI} (Appendix B, Equation 4.4). Hence, to map our probed points from the C reference frame to the reference frame I, we had to compute the inverse transformation from C to I (T_{IC}). Inverting a 4x4 transformation matrix is relatively trivial as the rotational component for the inverse is simply the transpose of the forward transformation.

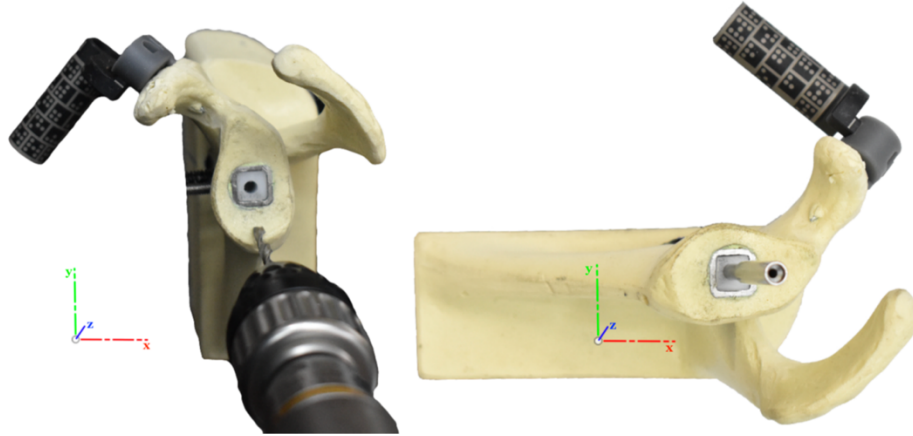


Figure 3.10: Drilling orientation during the mock trials (left) had the implant reference frame oriented such that the positive y-axis was directed in the anatomically superior direction. While probing (right) the implant reference frame was rotated 90°, such that the positive x-axis was directed in the anatomically superior direction.

3.8 Calculating Trajectory Angulation

After applying all of the transforms to the set of probed points to represent them in the reference frame I, we were able to compute the angular and translational offsets between the pre-plan and the actual drilling results. To determine the location of the drilling entry point, we simply plotted the X and Y coordinates of all the entry hole points on a 2D graph.

To generate a line that defines the trajectory of the drill, we used the vector connecting the tip of the long pin and the entry hole. We had originally considered using the short pin as we were concerned that the entry hole might have chips on the edge which could affect repeatability. However, inspection of the drilled holes showed generally clean edges so we opted to use the entry hole in order to gain higher resolution in the angulation measurement as the distance between the long pin's tip and the entry hole was roughly 20mm greater than between the long and short pin tops. As shown in the Figure 3.11, we then calculated the angle of this vector in both version (θ) and inclination (β) relative to the pre-planned trajectory using trigonometry.

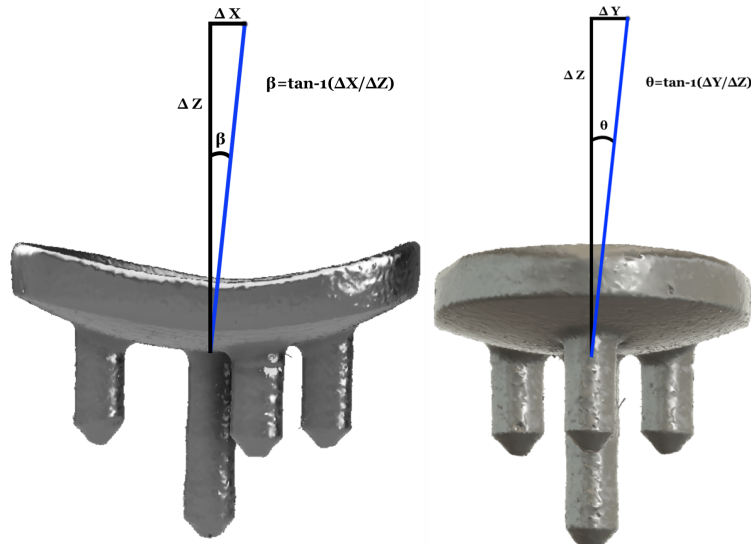


Figure 3.11: The trigonometry used to compute the angles θ and β by considering the offset between the origin and the point probed on the long pin. The two images above are rotated 90 degrees from one another, used to compute inclination (left) and version (right).

3.9 Drill Calibration

To check the orientation of the drill axis and the location of the drill tip relative to the marker array used on the drill handle, we used a calibration phantom from NST.

3.9.1 Physical Device

The phantom is a single-piece measurement tool that is part of the standard NST surgical system setup and is normally used to determine the location of the drill tip after mounting (since the process of mounting the drill in the chuck has some variability associated with it, especially in the axial direction since different-length drill bits may be used). This calibration phantom (Figure 3.12) is a block of stainless steel, with divots machined into it by a high-precision CNC machine at known locations relative to the datum, and later measured on a CMM to confirm accuracy. It accepts any of the NST patient trackers, and uses a kinematically-repeatable mount to attach them to the stainless-steel block. The offset between the patient tracker and any of the divots is established by construction and described in the engineering drawing below (Figure 3.13).

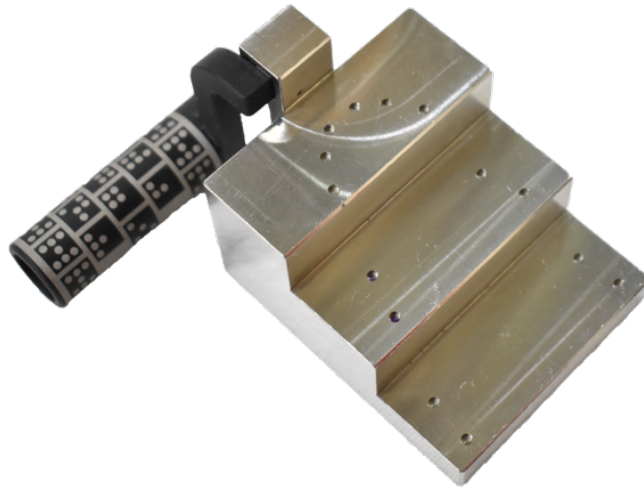


Figure 3.12: The calibration phantom is a block of stainless steel, with divots machined into it by a high-precision CNC machine at known locations relative to the datum, and later measured on a CMM to confirm accuracy. This device is used to ensure the calibration between a marker array, and the surgical drill which it is rigidly attached to.

3.9.2 Phantom Test Protocol

To perform the calibration, the surgical drill is held perpendicular to the divot of interest, allowing the software to collect the estimated drill tip positions 16 times per second. By holding the drill in place for a minute, roughly 960 data points are collected.

The average of these observed values was then subtracted from the values predicted by the model of the drill (which assumes that the drill tip is in line with the axis determined by the cylindrical feature of the handle to which the marker array is attached), to generate an offset between the predicted and measured locations of the drill tip. Any difference between these will mean that the measured hole locations are likely to be somewhat displaced from the originally-targeted locations.

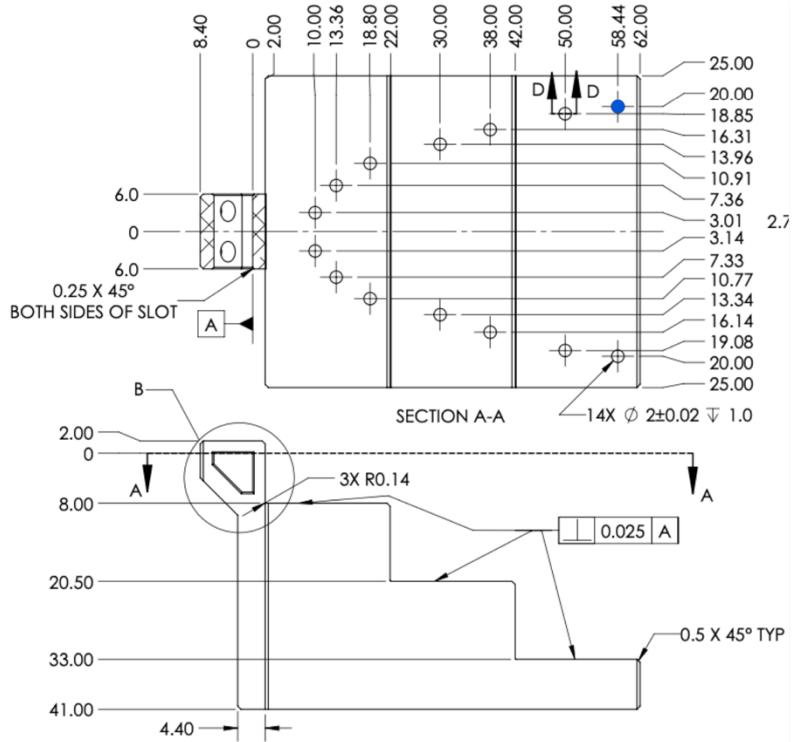


Figure 3.13: Engineering drawing of the phantom block, with construction specifications for all of the divots relative to the datum. A blue dot represents the divot we probed during our experimentation.

Chapter 4: Results

In this chapter we present the repeatability and accuracy results we found for the entry point as well as the trajectory angle of the drill bit relative to the pre-plan. We further delineate the results we observed for our variability source testing.

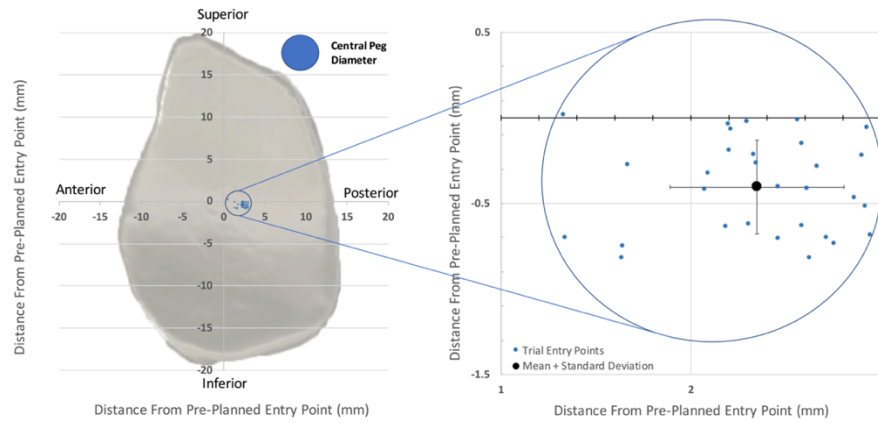
4.1 Entry Point Variability

Figure 4.1 shows the distribution of measured entry points for our three participants overlaid on a full-scale representation of the glenoid surface and the nominal targeted entry point at (0,0), while Table 4.1 presents the summary of descriptive statistics. There was an average bias across all participants of 2.46 mm in the AP direction and -0.09 mm in the SI direction. All individual standard deviations were below 0.5 mm.

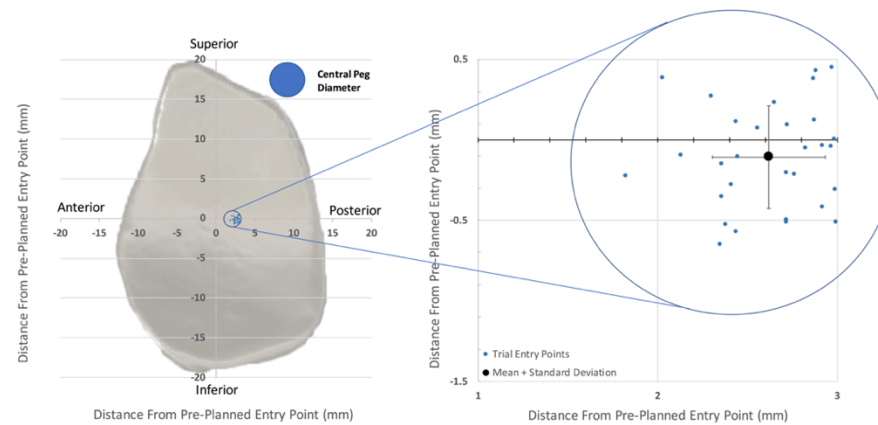
4.2 Trajectory Angulation Variability

Figure 4.2 shows the distribution of inclination and version angles by participant, as well as a perspective view of the distribution of executed trajectories (portraying both translational and angular variations). The average bias across all participants was 0.72° in version and -0.13° in inclination, with all standard deviations close to or below 1° .

Surgeon:



Fellow:



System Developer:

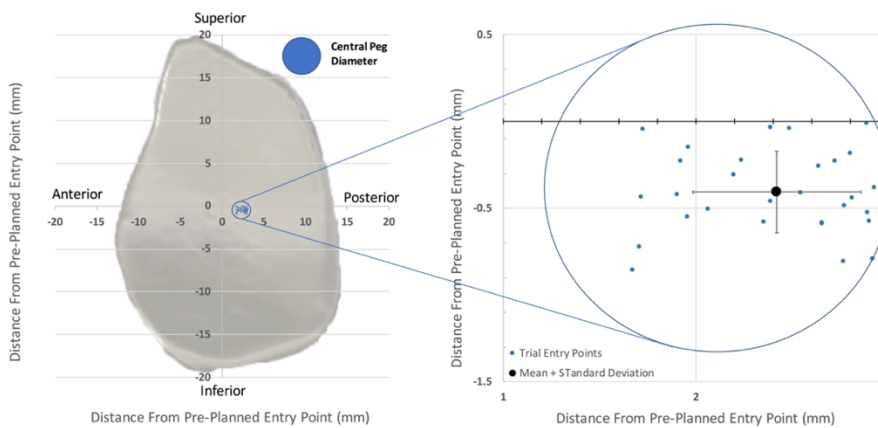
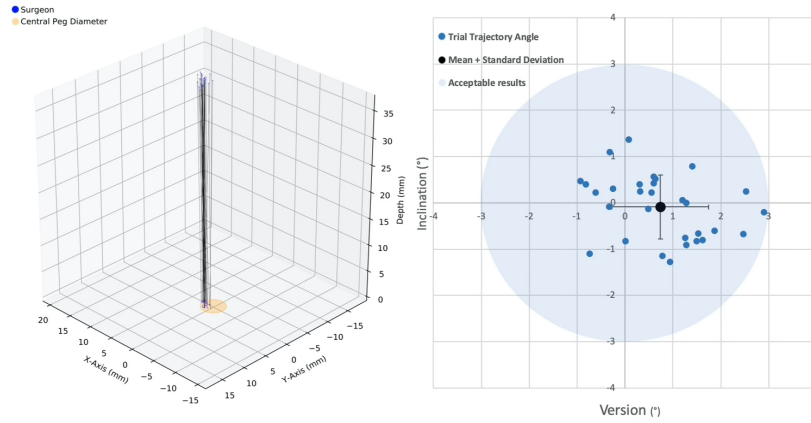
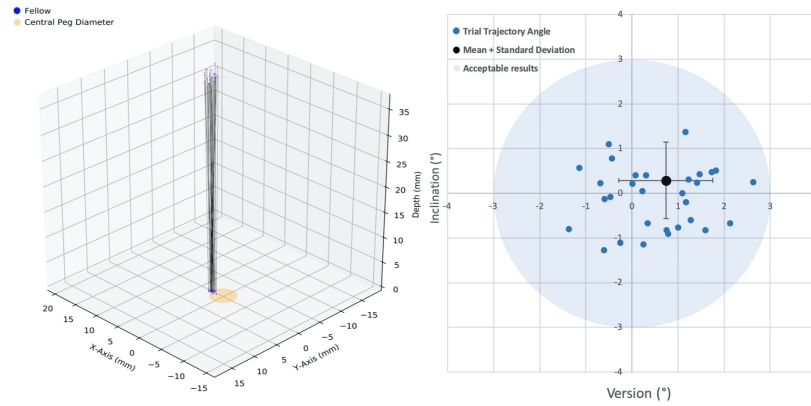


Figure 4.1: Entry hole locations of all thirty trials for each participant relative to the pre-plan target of (0, 0). A size reference for the central peg diameter (4.4mm) is shown as a dark blue filled circle, as well as the glenoid dimensions (in grey). The faint blue circle outline in the plots to the right has a radius of 900 microns and illustrates that all trial points for each participant fit within this sub-millimetric area.

Surgeon:



Fellow:



System Developer:

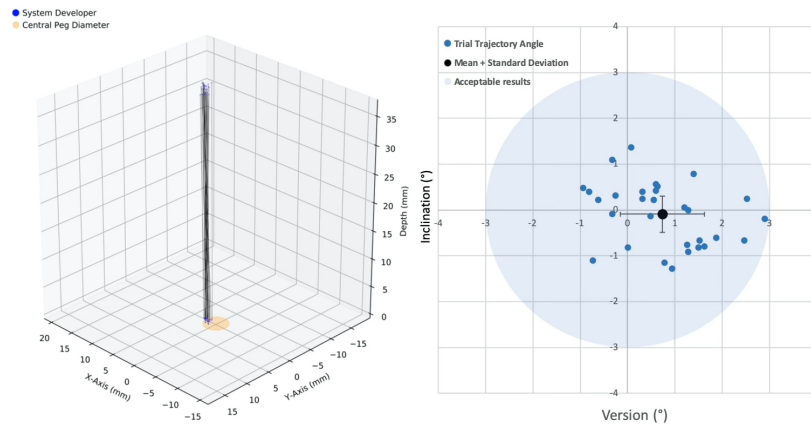


Figure 4.2: The distribution of executed trajectories (left column) and angular deviations for version and inclination (right column). The top cluster of points in each plot on the left indicates the measured locations of the top pins, while the bottom cluster indicates the measured locations of the entry holes. A size reference for the central peg diameter is indicated by the light orange circles. The faint blue circles have a radius of 3°, which approximates the variability reported for version achieved by the Exactech surgical navigation system (Nashikkar 2019).

	Surgeon	Fellow	System Developer
Entry Point: Anterior-posterior	2.35 ± 0.46mm CI: 0.37 - 0.62mm	2.62 ± 0.31mm CI: 0.25 - 0.42mm	2.42 ± 0.44mm CI: 0.35 - 0.59mm
Entry Point: Superior-inferior	-0.40 ± 0.27mm CI: 0.22 - 0.36mm	-0.11 ± 0.32 mm CI: 0.25 - 0.43mm	0.24 ± -0.41mm CI: 0.33 - 0.55mm
Angulation: Version	0.74° ± 1.01° CI: 0.80 - 1.36°	0.55° ± 1.02° CI: 0.81 - 1.37°	0.87° ± 0.89° CI: 0.71 - 1.20°
Angulation: Inclination	-0.09° ± 0.69° CI: 0.55 - 0.93°	-0.16° ± 0.86° CI: 0.68 - 1.16°	-0.15° ± 0.39° CI: 0.31 - 0.52°

Table 4.1: Means and standard deviations of the observed entry point location and angulation for the drill trajectory relative to the predefined plan at X0, Y0, θ=0, β=0 by participant and 95% confidence intervals for precision.

4.3 Variability Attributable to Aspects of Experiment Design

Some of the variability reported above could potentially be attributable to some aspects of our experimental pipeline. In this section, we estimate the potential contributions of two factors: (1) extraction and re-insertion of the plastic drilling specimens and (2) the drilling process itself. To assess the variability caused by reinserting the plastic into the metal tube, we inserted the long pin into a single specimen, and then removed and reinserted this single specimen 30 times. We probed the long pin for its location each time, and then evaluated the variability in resulting measurements. Table 4.2 shows the resulting standard deviations in X and Y. These transverse standard deviations (X and Y) were both markedly lower than the 0.24-0.46 mm values found for

the entry hole locations, so the reinsertion process appears to contribute negligible variability to the overall process. Variation in the Z direction has negligible effect on the transverse location of the entry hole, so is not presented.

X	Y
0.017	0.011

Table 4.2: The standard deviation in measuring the long pin’s hole location for all 30 trials.

To assess whether the process of drilling through the specimen could induce significant variability, we used a CNC machine to drill 30 individual specimens. We then placed each specimen in our measurement jig and measured the position of the top hole of the long pin. The resulting standard deviations are shown in Table 4.3. The transverse standard deviations are similar to one another (approximately 0.05 mm) and again only a small fraction of the 0.24-0.46 mm standard deviations found for the entry hole locations. While these values are larger than for measurement repeatability alone (about 0.01-0.02 mm), they are still small enough to conclude that the drilling process itself induces negligible variability in comparison with the user-related processes of targeting and drilling.

X	Y
0.051	0.056

Table 4.3: Shows the standard deviation measured for all 30 trials. This variability defines the variability in measurement + drilling. Here we can see that the variability we measured is negligible, especially compared to the other errors. Similarly, the error due to the process of drilling was also found to be modest relative to other sources of error.

4.4 Assessing Deviations from Plan

We noted above that there was a bias across the various participants with respect to the nominal target position of over 2 mm (primarily in the anterior direction) and almost 1 degree (primarily in version). This likely arises for two main reasons: (1) we only performed a nominal registration with the anatomic model (using a simple three-point registration scheme) because the anatomic model lacked the soft tissues, joint cartilage and other anatomical structures such as osteophytes that would need to be accommodated in a live surgical procedure, so using a more sophisticated registration scheme for the present study would lack realism and call any reported accuracy results into question, and (2) we did not calibrate the drill axis relative to the drill's marker pattern, so the drill tip and axis orientation may have deviated from the positions displayed on the navigation system.

To estimate the size of the latter effect (i.e., non-calibration of the drill), we performed the phantom calibration described in the previous chapter. Figure 4.3 shows a time series of data we recorded when holding the nominally-calibrated drill on a fixed location on the calibration phantom. The jitter levels on the measurements were low – on the order of +/- 0.1 mm.

While probing a point on the phantom with a known position of (20.00 mm, -58.44 mm, -31.88 mm) in the phantom's reference frame, we measured an average drill tip position of (17.78 ± 0.04 mm, -58.01 ± 0.04 mm, -32.19 ± 0.08 mm), which results in a deviation of (-2.22 mm, 0.43 mm, -0.31 mm) relative to the known locations. As illustrated in Figure 4.4, the dominant calibration error appears to be a leftward displacement of the tip.



Figure 4.3: Superior-inferior (top) and anterior-posterior (bottom) offset of drill tip over 941 samples (orange), relative to a predefined point on the calibration phantom (blue).

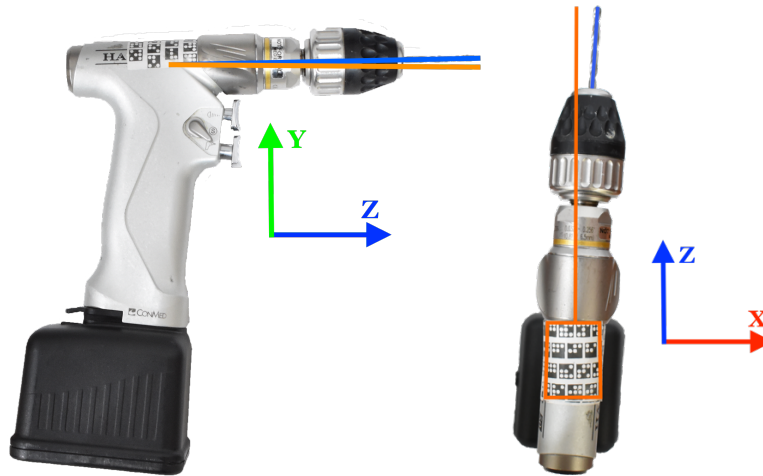


Figure 4.4: Sketch illustrating (exaggerated for effect) the deviation of the assumed drill tip location (orange, based on the central axis of the marker array) relative to the actual location (blue).

4.5 Qualitative feedback

Informally we provided the fellow and the surgeon with the opportunity to comment on the clinical practicality of the system that they used, and both reported that they expected it would be easy to use intraoperatively. The two key issues they identified were the following.

- The marker array needs to be placed somewhere other than the drill barrel.
- The drill bit used in surgery is much longer than the one used in the apparatus.

Chapter 5: Discussion

In this chapter we discuss the outcomes of our study and the significance of our results as they relate to total shoulder arthroplasty. We also discuss the limitations of our process and offer suggestions for further development.

The purpose of this thesis was to investigate whether it is possible to create a practical workflow for total shoulder arthroplasty based on Navigate Surgical Technologies' relatively unobtrusive tracker technology which demonstrates acceptable targeting performance. We succeeded in setting up a clinical configuration for TSA in which the shoulder, the cameras and other required components are all in clinically-realistic positions, and demonstrating across three subjects with very different levels of surgical expertise that they were all able to execute a planned surgical trajectory with high precision on a synthetic anatomical model.

The entry point precision amongst all thirty results for each participant was below 0.5 mm for all three participants (surgeon, fellow) and system developer) in both the anterior-posterior and superior-inferior directions. Similarly, the angular precision was approximately 1 degree or less for all participants in both version and inclination. With sub-millimetre precision for the drilling of the entry hole, as well as a standard deviation of less than roughly one degree in angular deviation for all participants, these values are markedly lower than the whole-system precisions shown in Figure 1.9. Hence, the primary conclusion of this study is that a navigation system for TSA built on Navigate Surgical's marker technology can likely provide high precision during the targeting phase of a navigated procedure.

5.1 Study Limitations

In this section we discuss three significant limitations of this study.

5.1.1 Tracker Registration

As explained in section 2.8, we have not implemented a realistic registration process that would be suitable for use on cadaveric specimens or patients. Instead, we implemented only a basic three-matched-points registration algorithm because we were working with a synthetic anatomical model which did not accurately capture all of the considerations that would be present in a real clinical situation. These considerations are related primarily to anatomical factors such as the presence of cartilage, osteophytes, soft tissue, and other aspects of the surgical exposure. Hence, we chose not to implement a registration technique of greater complexity, as our outcomes would not have been realistic regardless.

In addition, during this initial development we were working with the NST software, where we were further constrained to work with the workflows built into their system. In their normal application to dental surgery, registration is conducted automatically through use of fiducial markers which are present during the CT scanning process, which eliminates the requirement for a separate registration tool or intraoperative registration protocol. However, since our protocol was based on use of a pre-existing CT scan in which there are no fiducial markers present, the only practical registration technique available to us was the 3-point paired point registration scheme provided in the NST software. We therefore used this registration technique primarily to place the drilling target in a nominally realistic position for use in the targeting study. We specifically did not intend to assess overall system accuracy at this stage, so did not require a more accurate registration step. Such an algorithm would only be required at the later stages of cadaveric or patient testing.

5.1.2 Tool Calibration

Similarly, since we already knew that our primary evaluation criterion at this stage of development was going to be targeting precision, we did not need to accurately calibrate the drill axis. Rather, we simply needed a nominal estimate of where the drill axis was, and as long as this was maintained constant throughout the experiments, we would be able to evaluate precision. Hence, we did not develop nor implement a drill axis calibration technique, although such algorithms are available in the literature. We did, however, perform an evaluation using the phantom test model as described in our methods (section 3.9) to determine where the tip of the tool was relative to the assumed tip position. This enabled us to estimate that the calibration process was out by approximately 2.3mm (section 4.4), which is similar to the error we found in the drill entry point results, where the average for all three participants was $2.46\text{mm} \pm 0.71\text{mm}$. Furthermore, the error induced by the drill tip malposition was in the opposite direction from the offsets we observed, which was as expected. As shown in Figure 5.1, when we probed the divot in the phantom model, we placed the true drill tip on the known divot, and the expected drill tip was shown by the system to be 2.22mm to the left of the true location. When we conducted the drilling in the bone, we were placing the assumed tip location on the desired entry hole location on the bone, but the actual holes were drilled an average of 2.46mm to the right. Given the close correspondence between the drill axis calibration error and the measured average location of the entry holes, we believe that properly calibrating the marker array to the drill axis would enable us to substantially correct this offset observed in the results.

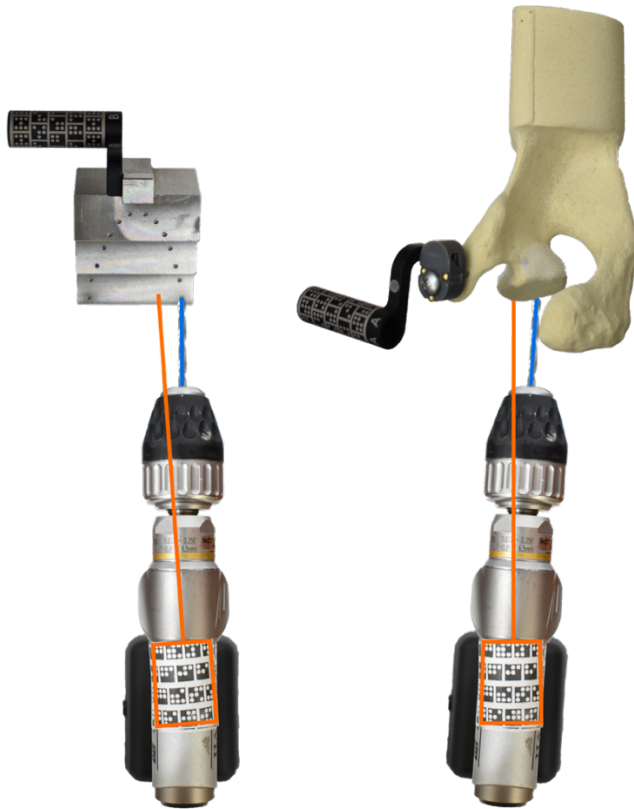


Figure 5.1: Possible explanation of medial lateral bias in entry hole location (deviations exaggerated for clarity). In the diagrams above, the blue line represents the actual location of the drill, whereas the orange line represents the assumed drill axis based on the center of the cylindrical shell formed by the tracking array. Note that the measured offset corresponds to a rightward displacement of the drilled hole relative to the position indicated on the targeting display.

5.1.3 Extending Drill Length and Increasing Camera Field of View

During our system development, we had to accommodate some limitations of the present NST system. In particular, we had to use a shorter drill bit than what is normally used during a TSA. We did this because the field of view (FOV) of the NST cameras currently being used was designed to accommodate the smaller drills used in dental surgery and so is a little constrained for our application. Before using the NST-based system in surgery, we will have to modify the field of view to accommodate the drill bit that is typically used. In the current dental application, the two marker arrays are no more than 17cm apart during drilling. In contrast, the TSA application

requires a field of view that would capture both marker arrays at a working distance of approximately 40cm from each other. To capture both the patient tracker and drill marker array using the standard TSA drill bit, we would need to increase the size of the working volume by a factor of roughly 2.5. To do this, we might expand the field of view of the cameras, which would decrease the resolution (measured in pixel/mm) by a similar factor. The current nominal resolution of the system is approximately ~ 5 pixels/mm (~ 0.17 mm/pixel, based on the current 1080p sensor) with the nominal field of view used in this study, so, absent any changes in the camera sensor itself, this would be reduced to ~ 2.5 pixels/mm (~ 0.35 mm/pixel). If we were to simply expand the camera's field of view, then the system accuracy could potentially be degraded to a detectable level in the resulting navigation system. It might therefore be advisable to replace the cameras with higher resolution sensors (eg, moving from a 1k to a 2k or 4k sensor). In addition, we could increase the size of the marker array used on the drill by a factor of approximately 2, which would keep the angular resolution approximately constant. In any case, the overall accuracy of the system is still likely governed by the accuracy of the registration and tool calibration steps, so the overall impact on the procedure accuracy may be negligible.

5.1.4 Plastic Inserts

The Delrin plastic used for the trial inserts machined nicely, but did not necessarily replicate the drilling characteristics of bone. While Delrin is more uniform than bone, we were unable to characterize this difference. We assume it had no effect on the initial alignment of the surgical tool with respect to the entry point, but we did not account for how this uniform density may have affected the drilling trajectory during the drilling process of our trials. However, we have no strong reason to believe that the effects would be significant.

5.2 Discussion of System Performance

Our most important finding from this experiment was that our end-to-end targeting precision for locating the entry hole was sub-millimetric, and the standard deviation in angular variation across all participants was only about one degree. These precision results reflect all contributors to variation that arise after the drilling target has been identified, including variability in marker tracking and human-related tasks such as aligning the drill axis and following the drilling trajectory, as well as the measurement processes. As expected, the measurement repeatability showed the lowest standard deviation. The step of drilling with a jig incorporated both drilling and measurement, so in principle the variance should be greater than the measurement repeatability alone, which was confirmed. However, this variability was much lower than the overall variability that we found in the user study. This demonstrates that neither the drilling nor the measurement process introduced any significant variability, which suggests that the bulk of the variability found in our user study arises from the variability associated with users performing the targeting and drilling tasks. The precision results we found were broadly consistent across the three users who performed the study. Since only three users were involved in this study, we cannot conclude that the results we obtained would necessarily hold across all possible users of the system, the fact that users with markedly different levels of surgical experience were able to use the system equally well suggests that results in practice are not likely to depend significantly on the surgical experience of the users.

Our results for angular repeatability in targeting were markedly lower than the overall procedure results obtained using the conventional freehand surgical methods. With angular deviations of roughly 11° (Gregory 2013), 7° (Nashikar 2019), and 8° (Throckmorton 2015), the procedure variance of the freehand method is approximately 10x larger than our system's targeting

repeatability. We therefore conclude that as long as the registration and calibration variances end up being reasonably low, a navigation system built on the NST technology should be able to demonstrate better overall variability than freehand procedures.

With reference to previous navigation systems, our angular repeatability results were markedly more precise than results reported by Wang (2019) and Nashikkar (2019), both of whom studied the accuracy and precision of the ExactechGPS Shoulder Application system. Wang found angular standard deviations of 2° in version and 3° in inclination, while Nashikkar found angular standard deviations of 2.8° in version and 4.8° in inclination. Neither reported either accuracy or precision in locating the entry hole. However, while the precision we found was substantially lower than that reported in these two studies, it reflects only the variability associated with the targeting process, whereas Wang and Nashikkar reported end-to-end variability for the entire surgical process, including the registration step which we did not address in our study. Nonetheless, since the angular variance we found was on the order of about 10-25% of the variances reported by these other authors, it is reasonable to speculate that the variance associated with registration is likely the dominant contributor to the end-to-end variances reported in these studies and therefore that using the NST system in place of conventional optical tracking will likely not lead to end-to-end variance larger than what they have reported.

We can also compare our precision results with results reported for protocols using Patient-Specific Implants (PSI). The angular results found by Gauci (2016) were 5.1° in version and 5.3° in inclination, while Throckmorton (2015) found similar results of 4.8° and 4.3° in version and inclination respectively. The results from these two studies are markedly larger than both our system's targeting variability and that reported by Wang and Nashikkar for navigation systems. Both Gauci and Throckmorton also reported entry point repeatability with standard

deviation of about 2mm, which was approximately three times the targeting precision of our system in translation (an average of 0.65mm). Hence, our targeting variance was roughly 10% of the variance described by Gauci and Throckmorton, which in our view justifies further development of the NST-based system with the aim of incorporating a more appropriate registration process for use in cadaveric (and ultimately patient) studies.

In terms of the system feasibility, based on the qualitative results described in chapter 4, the general impression was that the system would be acceptable for clinical use but some modest changes might need to be made to the location of the marker array. The first suggestion was with regards to the placement of the marker array, and the problems that may arise if it is situated on the barrel of the drill. It was suggested that the barrel of the drill is where a surgeon would usually place their second hand in order to stabilize and support the drill. The second suggestion was to test the system with a longer drill bit as would be anticipated in a true surgical case. While the use of a longer drilling bit may prompt issues with the camera's field of view as described in section 5.1.3 above, it is unlikely to add error once the drilling has begun. This is because once the drill bit is in contact with the bone, the longer lever arm means that small unintentional movements of the drill will result in smaller angular variation in the drilling trajectory.

5.3 Recommendations for Moving Towards Clinical Testing

While we have demonstrated excellent targeting repeatability for our system, it will be necessary to add an appropriate registration method and assess the system's overall accuracy, before deploying the system clinically because there is significant uncertainty regarding the repeatability of the registration step that would be needed in a clinical application (which arises from the presence of soft tissue in live patients). Similarly, a tool calibration protocol must be

implemented and evaluated. NST has a protocol in place to generate configuration files for each individual dental surgical tool with a marker array applied to it. It would be of great benefit to modify this process and apply it to the larger drill used in TSA.

Finally, the FOV problem has to be solved before this system can be comfortably used with the proper length drill. I would recommend discussing a possible fix for this problem with the team at NST as it will likely require modifications to the design of the base holding the stereo camera pair.

5.4 Concluding Remarks

In this study, we have demonstrated that it is indeed possible to create a workflow for total shoulder arthroplasty based on Navigate Surgical Technologies' relatively unobtrusive tracker technology that supports excellent precision during the targeting and drilling phase of the surgery. The design of our system and the associated components addresses many of the anticipated challenges that would arise in implementing this new curved marker array technology for shoulder replacement surgery. Indications from our literature review suggest that the obtrusiveness of current navigation systems has resulted in a reduced adoption rate for this technology, despite its demonstrated ability to produce more accurate and precise positioning of implants. We speculate that by pursuing development of a TSA navigation based on this newer and less obtrusive marker technology could improve the uptake rates of surgical navigation for TSA in future, and perhaps be applied to other surgical navigation applications as well.

Bibliography

- Adams JE, Sperling JW, Hoskin TL et al (2006) Shoulder arthroplasty in Olmsted County, Minnesota, 1976–2000: a population-based study. *J Shoulder Elbow Surg* 15:50–55. doi:10.1016/j.jse.2005.04.009
- Antuna, S. A., Sperling, J. W., Cofield, R. H., & Rowland, C. M. (2001). Glenoid revision surgery after total shoulder arthroplasty. *Journal of Shoulder and Elbow Surgery*, 10(3), 217-224. doi:10.1067/mse.2001.113961
- Bellemans, J. (2009). Navigation and CAS: is D-day approaching? *Knee Surgery, Sports Traumatology, Arthroscopy : Official Journal of the ESSKA*, 17(10), 1141–2.
- Bishop, J. L., Kline, S. K., Aalderink, K. J., Zauel, R., & Bey, M. J. (2009). Glenoid inclination: In vivo measures in rotator cuff tear patients and associations with superior glenohumeral joint translation. *Journal of Shoulder and Elbow Surgery*, 18(2), 231-236. doi:10.1016/j.jse.2008.08.002
- Boddapati, V., Fu, M. C., Schairer, W. W., Gulotta, L. V., Dines, D. M., & Dines, J. S. (2017). Revision Total Shoulder Arthroplasty is Associated with Increased Thirty-Day Postoperative Complications and Wound Infections Relative to Primary Total Shoulder Arthroplasty. *HSS Journal* ®, 14(1), 23-28. doi:10.1007/s11420-017-9573-5
- Bohsali KI, Wirth MA, Rockwood C A., Jr Complications of total shoulder arthroplasty. *J Bone Joint Surg (Am)* 2006;88(10):2279–92.
- Boileau P, Avidor C, Krishnan SG, Walch G, Kempf JF, Mole D. (2002) Cemented polyethylene versus uncemented metal-backed glenoid components in total shoulder arthroplasty: a prospective, double-blind, randomized study. *J Shoulder Elbow Surg* 11:351-9.
- Bouras, T., Bitas, V., Fennema, P., & Korovessis, P. (2015). Good long-term results following cementless TKA with a titanium plasma coating. *Knee Surgery, Sports Traumatology, Arthroscopy*, 25(9), 2801-2808. doi:10.1007/s00167-015-3769-3
- Braun, S., Schroeder, S., Mueller, U., Sonntag, R., Buelhoff, M., & Kretzer, J. P. (2018). Influence of joint kinematics on polyethylene wear in anatomic shoulder joint arthroplasty. *Journal of Shoulder and Elbow Surgery*, 27(9), 1679-1685. doi:10.1016/j.jse.2018.02.063
- Chandler JW, Williams GR Jr. Surgical approach and techniques for total shoulder arthroplasty: tips and tricks. *Instr Course Lect*. 2011;60:91–7.
- Chow, J. C., & Torre, P. K. (2016). Patient-Specific Total Knee Arthroplasty. *Minimally Invasive Surgery in Orthopedics*, 1319-1332. doi:10.1007/978-3-319-34109-5_124

- Cvetanovich, G. L., Naylor, A. J., Obrien, M. C., Waterman, B. R., Garcia, G. H., & Nicholson, G. P. (2020). Anatomic total shoulder arthroplasty with an inlay glenoid component: Clinical outcomes and return to activity. *Journal of Shoulder and Elbow Surgery*, *29*(6), 1188-1196. doi:10.1016/j.jse.2019.10.003
- Farmer, Kevin, Hammond, Jason, Queale, William, S MD, MS, Keyurapan, Ekavit & McFarland, Edward. (2007). Shoulder Arthroplasty versus Hip and Knee Arthroplasties: A Comparison of Outcomes. *Clinical Orthopaedics & Related Research*, *455*, 183-189. <https://doi.org/10.1097/01.blo.0000238839.26423.8d>
- Farron A, Terrier A, Buchler P. Risks of loosening of a prosthetic glenoid implanted in retroversion. *J Shoulder Elbow Surg*. 2006;*15*(4):521–6
- Friedman, R. J., Cheung, E., Grey, S. G., Flurin, P., Wright, T. W., Zuckerman, J. D., & Roche, C. P. (2019). Clinical and radiographic comparison of a hybrid cage glenoid to a cemented polyethylene glenoid in anatomic total shoulder arthroplasty. *Journal of Shoulder and Elbow Surgery*, *28*(12), 2308-2316. doi:10.1016/j.jse.2019.04.049
- Friedman, R. J., Hawthorne, K. B., & Genez, B. M. (1992). The use of computerized tomography in the measurement of glenoid version. *Journal of Bone and Joint Surgery. American Volume*, *74*(7), 1032.
- Gartsman GM, Elkousy HA, Warnock KM, Edwards TB, O'Connor DP. Radiographic comparison of pegged and keeled glenoid components. *J Shoulder Elbow Surg* 2005;*14*:252-7.
- Gauci, M. O., Boileau, P., Baba, M., Chaoui, J., & Walch, G. (2016). Patient-specific glenoid guides provide accuracy and reproducibility in total shoulder arthroplasty. *The Bone & Joint Journal*, *98-B*(8), 1080-1085. doi:10.1302/0301-620x.98b8.37257
- Gori, M. D., Adamczewski, B., & Jenny, J. (2017). Value of the cumulative sum test for the assessment of a learning curve: Application to the introduction of patient-specific instrumentation for total knee arthroplasty in an academic department. *The Knee*, *24*(3), 615-621. doi:10.1016/j.knee.2017.03.007
- Gregory, T. M., Sankey, A., Augereau, B., Vandenbussche, E., Amis, A., Emery, R., & Hansen, U. (2013). Accuracy of Glenoid Component Placement in Total Shoulder Arthroplasty and Its Effect on Clinical and Radiological Outcome in a Retrospective, Longitudinal, Monocentric Open Study. *PLoS ONE*, *8*(10). doi: 10.1371/journal.pone.0075791
- Habermeyer P, Magosch P, Luz V, Lichtenberg S. Three-dimensional glenoid deformity in patients with osteoarthritis: a radiographic analysis. *J Bone Joint Surg (Am)* 2006;*88*(6):1301–7

- Heylen, S., Haver, A. V., Vuylsteke, K., Declercq, G., & Verborgt, O. (2016). Patient-specific instrument guidance of glenoid component implantation reduces inclination variability in total and reverse shoulder arthroplasty. *Journal of Shoulder and Elbow Surgery*, 25(2), 186-192. doi:10.1016/j.jse.2015.07.024
- Healy WL, Iorio R, Lemos MJ. Athletic activity after joint replacement. *Am J Sports Med*. 2001;29:377-388
- Hollatz, M. F., & Stang, A. (2014). Nationwide shoulder arthroplasty rates and revision burden in Germany: Analysis of the national hospitalization data 2005 to 2006. *Journal of Shoulder and Elbow Surgery*, 23(11). doi:10.1016/j.jse.2013.12.008
- Hopkins AR, Hansen UN, Amis AA, Emery R. The effects of glenoid component alignment variations on cement mantle stresses in total shoulder arthroplasty. *J Shoulder Elbow Surg* 2004;13:668-75.
- Huri, G., Familiari, F., Moon, Y. L., Doral, M. N., & Muccioli, G. M. (2020). *Shoulder arthroplasty: The Shoulder Club guide*. Cham, Switzerland: Springer.
- Hwang, Y., Kang, S., & Kim, H. (2019). Errors according to the number of registered markers used in navigation-assisted surgery of the mandible. *Head & Face Medicine*, 15(1). doi:10.1186/s13005-019-0190-z
- Jain NB, Higgins LD, Guller U et al (2006) Trends in the epidemiology of total shoulder arthroplasty in the United States from 1990–2000. *Arthritis Rheum* 55:591–597. doi:10.1002/art.22102
- Junnila, M., Laaksonen, I., Eskelinen, A., Pulkkinen, P., Havelin, L. I., Furnes, O., . . . Mäkelä, K. T. (2016). Implant survival of the most common cemented total hip devices from the Nordic Arthroplasty Register Association database. *Acta Orthopaedica*, 87(6), 546-553. doi:10.1080/17453674.2016.1222804
- Kircher J, Wiedemann M, Magosch P, et al. Improved accuracy of glenoid positioning in total shoulder arthroplasty with intraoperative navigation: a prospective-randomized clinical study. *J Shoulder Elbow Surg* 2009;18:515-20
- Koch, P. P., Miller, D., Pisan, M., & Fucentese, S. F. (2013). Radiographic accuracy in TKA with a CT-based patient-specific cutting block technique. *Knee Surgery, Sports Traumatology, Arthroscopy*, 21(10), 2200-2205. doi: 10.1007/s00167-013-2625-6
- Lazarus MD, Jensen KL, Southworth C, Matsen FA 3rd. The radio- graphic evaluation of keeled and pegged glenoid component insertion. *J Bone Joint Surg Am* 2002;84:1174-82.
- Martin, S. D., Zurakowski, D., & Thornhill, T. S. (2005). Uncemented Glenoid Component In Total Shoulder Arthroplasty. *The Journal of Bone and Joint Surgery-American Volume*, 87(6), 1284-1292. doi:10.2106/00004623-200506000-00014

- Merolla, G., Amore, B., Paladini, P., Cavagna, E., & Porcellini, G. (2013). Computed tomography quantification of bone density adjacent to cemented pegged polyethylene glenoid components in shoulder arthroplasty. *European Journal of Orthopaedic Surgery & Traumatology*, *24*(5), 753-761. doi:10.1007/s00590-013-1368-x
- Mezger, U., Jendrewski, C., & Bartels, M. (2013). Navigation in surgery. *Langenbecks Archives of Surgery*, *398*(4), 501-514. doi:10.1007/s00423-013-1059-4
- Nashikkar, P. S., Scholes, C. J., & Haber, M. D. (2019). Computer navigation re-creates planned glenoid placement and reduces correction variability in total shoulder arthroplasty: An in vivo case-control study. *Journal of Shoulder and Elbow Surgery*, *28*(12). doi:10.1016/j.jse.2019.04.037
- Page, R. S., Pai, V., Eng, K., Bain, G., Graves, S., & Lorimer, M. (2018). Cementless versus cemented glenoid components in conventional total shoulder joint arthroplasty: analysis from the Australian Orthopaedic Association National Joint Replacement Registry. *Journal of Shoulder and Elbow Surgery*, *27*(10), 1859–1865. doi: 10.1016/j.jse.2018.03.017
- Ricchetti, E. T., Jun, B.-J., Jin, Y., Entezari, V., Patterson, T. E., Derwin, K. A., & Iannotti, J. P. (2020). Three-Dimensional Computed Tomography Analysis of Pathologic Correction in Total Shoulder Arthroplasty Based on Severity of Preoperative Pathology. *Journal of Shoulder and Elbow Surgery*. doi:10.1016/j.jse.2020.07.033
- Sager, B. W., & Khazzam, M. (2018). Surgical Approaches in Shoulder Arthroplasty. *Advances in Shoulder Surgery*. doi:10.5772/intechopen.70363
- Schwartz, B. E., Savin, D. D., Youderian, A. R., Mossad, D., & Goldberg, B. A. (2014). National trends and perioperative outcomes in primary and revision total shoulder arthroplasty. *International Orthopaedics*, *39*(2), 271-276. doi:10.1007/s00264-014-2614-5
- Shapiro TA, McGarry MH, Gupta R, Lee YS, Lee TQ. Biomechanical effects of glenoid retroversion in total shoulder arthroplasty. *J Shoulder Elbow Surg*. 2007;16:S90–5
- Strauss, E. J., Roche, C., Flurin, P., Wright, T., & Zuckerman, J. D. (2009). The glenoid in shoulder arthroplasty. *Journal of Shoulder and Elbow Surgery*, *18*(5), 819-833. doi:10.1016/j.jse.2009.05.008
- Szabo I, Buscayret F, Edwards TB, Nemoz C, Boileau P, Walch G. Radiographic comparison of flat-back and convex-back glenoid components in total shoulder arthroplasty. *J Shoulder Elbow Surg* 2005;14:636-42.
- Szerlip B, Muh S, Streit J, Gobezie B. Glenoid exposure: tricks of the trade. *Semin Arthroplasty*. 2012;23:95–8.

- Theopold, J., Pieroh, P., Henkelmann, R., Osterhoff, G., & Hepp, P. (2019). Real-time intraoperative 3D image intensifier-based navigation in reversed shoulder arthroplasty—analyses of image quality. *BMC Musculoskeletal Disorders*, *20*(1). doi:10.1186/s12891-019-2657-2
- Thienpont E, Paternostre F, Van Wymeersch C. The indirect cost of Patient-Specific Instruments. *Acta Orthop Belg*. 2015 Sep;*81*(3):462-70. PMID: 26435242.
- Throckmorton, T. W., Gulotta, L. V., Bonnarens, F. O., Wright, S. A., Hartzell, J. L., Rozzi, W. B., Sperling, J. W. (2015). Patient-specific targeting guides compared with traditional instrumentation for glenoid component placement in shoulder arthroplasty: A multi-surgeon study in 70 arthritic cadaver specimens. *Journal of Shoulder and Elbow Surgery*, *24*(6), 965-971. doi:10.1016/j.jse.2014.10.013
- Trofa D, Rajae SS, Smith EL (2014) Nationwide trends in total shoulder arthroplasty and hemiarthroplasty for osteoarthritis. *Am J Orthop Belle Mead NJ* *43*:166–172
- Ungi T, Lasso A, Fichtinger G. Open-source platforms for navigated image-guided interventions. *Med Image Anal*. 2016 Oct;*33*:181-6. doi: 10.1016/j.media.2016.06.011.
- Villatte, G., Muller, A.-S., Pereira, B., Mulliez, A., Reilly, P., & Emery, R. (2018). Use of Patient-Specific Instrumentation (PSI) for glenoid component positioning in shoulder arthroplasty. A systematic review and meta-analysis. *Plos One*, *13*(8). doi: 10.1371/journal.pone.0201759
- Virani, N. A., Williams, C. D., Clark, R., Polikandriotis, J., Downes, K. L., & Frankle, M. A. (2013). Preparing for the bundled-payment initiative: The cost and clinical outcomes of total shoulder arthroplasty for the surgical treatment of glenohumeral arthritis at an average 4-year follow-up. *Journal of Shoulder and Elbow Surgery*, *22*(12), 1601-1611. doi:10.1016/j.jse.2012.12.028
- Wang, A. W., Wang, A. W., Hayes, A., Gibbons, R., & Mackie, K. E. (2019). Computer navigation of the glenoid component in reverse total shoulder arthroplasty: A clinical trial to evaluate the learning curve Elsevier. doi:10.1016/j.jse.2019.08.012
- Watkins, R. G., Gupta, A., & Watkins, R. G. (2010). Cost-Effectiveness of Image-Guided Spine Surgery. *The Open Orthopaedics Journal*, *4*(1), 228-233. doi:10.2174/1874325001004010228
- Wong, R., Jivraj, J., & Yang, V. (2014). Current limitations and opportunities for surgical navigation. *University of Toronto Medical Journal*, *92*(1), 7-9.
- Yongpravat, C., Kim, H. M., Gardner, T. R., Bigliani, L. U., Levine, W. N., & Ahmad, C. S. (2013). Glenoid implant orientation and cement failure in total shoulder arthroplasty: a finite element analysis. *Journal of Shoulder and Elbow Surgery*, *22*(7), 940–947. doi: 10.1016/j.jse.2012.09.007

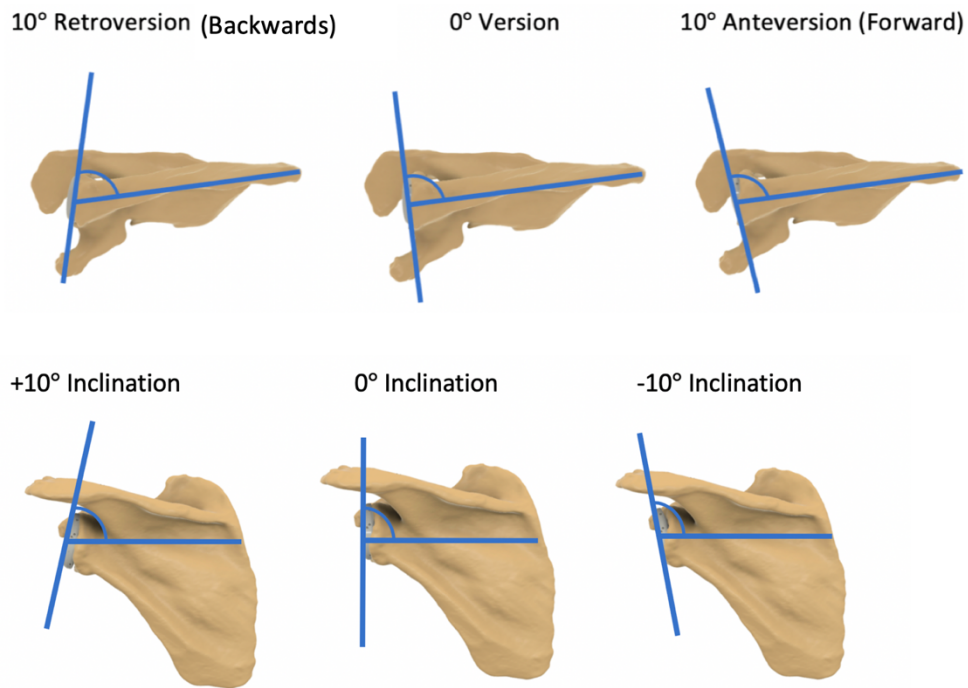
Yuan, 黄 H., Feipeng, 达 D., & Haiji, 陶 T. (2015). An Automatic Registration Algorithm for Point Cloud Based on Feature Extraction. *Chinese Journal of Lasers*, 42(3), 0308002. doi:10.3788/cjl201542.0308002

Zmistowski, Benjamin, Padegimas, Eric, Howley, Michael, PA-C, PhD, Abboud, Joseph, Williams, Gerald, et al. (2018). Trends and Variability in the Use of Total Shoulder Arthroplasty for Medicare Patients. *Journal of the American Academy of Orthopaedic Surgeons*, 26, 133-141. <https://doi.org/10.5435/JAAOS-D-16-00720>

Appendices

Appendix A - Measuring Procedural Success

Glenoid implant positioning is usually characterized using two angles: version and inclination. Version refers to the forward and backwards angulation of the glenoid relative to the scapula. An anterior facing glenoid is said to be anteverted, while a posteriorly facing glenoid is retroverted. Similarly, inclination is defined as the angulation of the glenoid relative to the scapula in the up and down direction. A glenoid facing superiorly has positive inclination, while an inferior facing glenoid is negatively inclined.



To identify the desired version and inclination of the implantable component, pre-operative planning is used. Here, the targeted trajectory axis is defined using a pre-operative CT scan. Post-operatively, the position of the implanted devices is evaluated using X-rays, as CT images are not

routinely acquired post-operatively due to the greater radiation doses involved, as well as the expense (Ricchetti, 2020).

To measure the version of a glenoid on a trans-axillary shot, Friedman (1992) introduced the Friedman line, which runs along the scapular axis from the medial tip of the scapula to the center of the glenoid fossa. The version is then computed to be the difference in angles between the scapular axis line and a line along the edges of the glenoid fossa, relative to the perpendicular line (Figure 6.1).

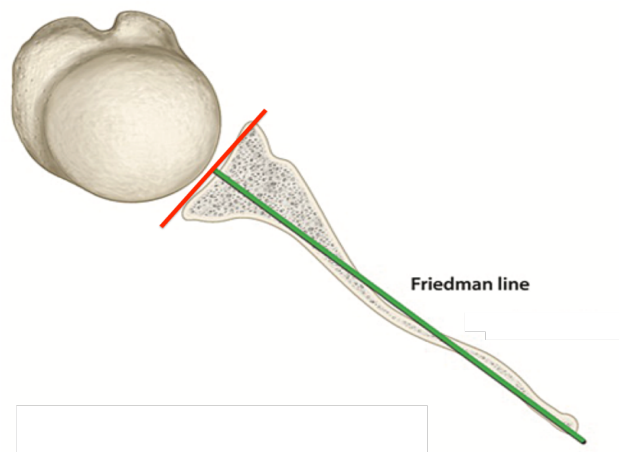


Figure 6.1: The Friedman line (green) is found by drawing a line from the tip of scapular body to center of articular surface. A perpendicular line (red) drawn at the articular surface depicts the desired glenoid angle. Adapted from "The use of computerized tomography in the measurement of glenoid version" by Friedman, R. J., (1992) *Journal of Shoulder and Elbow Surgery*, American Volume, 74(7).

Similarly, anatomic landmarks can be identified to generate the ideal trajectory axis for inclination (Figure 6.2). This ideal inclination is defined as the angle between two lines. The first is the line formed by connecting the point found at the intersection of the scapular spine and the medial border (Figure 6.2, point A) to the spinoglenoid notch (Figure 6.2, point B) (Bishop *et al.* 2009). The second line is found connecting the superior glenoid rim (Figure 6.2, point C) and inferior glenoid rim (Figure 6.2, point D) (Bishop *et al.* 2009).

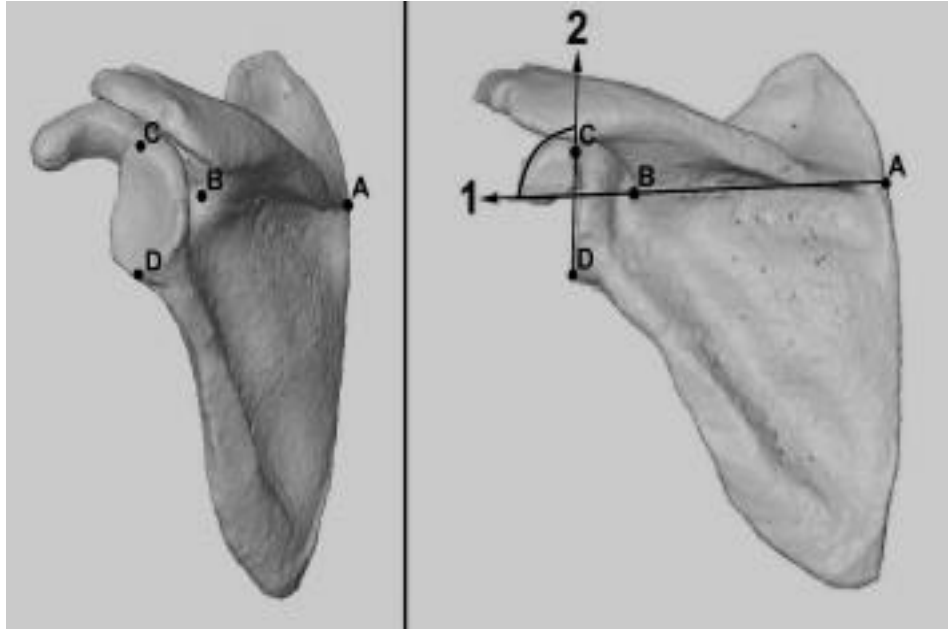


Figure 6.2: Landmark points on scapula used to generate inclination trajectory. Adapted from "Glenoid Inclination: In-Vivo Measures in Rotator Cuff Tear Patients and Associations with Superior Glenohumeral Joint Translation" by Bishop, J.L., 2009, *Journal of Shoulder and Elbow Surgery*, 18(2). Copyright [2009] with permission from Elsevier.

Appendix B - Transform Matrix Equations

$$T_{s1p} = \begin{pmatrix} -0.03 & 1.00 & 0.00 & -27.99 \\ -0.98 & -0.03 & -0.19 & 76.78 \\ -0.19 & -0.01 & 0.98 & -27.72 \\ 0.00 & 0.00 & 0.00 & 1.00 \end{pmatrix}$$

Equation 4.1: This equation denotes the 4x4 transform matrix resulting from manual alignment of the probed points to the points defining the surface mesh.

$$T_{ss1} = \begin{pmatrix} 1.00 & -0.01 & 0.01 & 0.75 \\ 0.01 & 1.00 & 0.00 & -0.08 \\ 0.01 & 0.00 & 1.00 & 0.44 \\ 0.00 & 0.00 & 0.00 & 1.00 \end{pmatrix}$$

Equation 4.2: This equation denotes the 4x4 transform matrix resulting from the ICP registration of the two point-clouds. It describes the transform between the S1 reference frame and S.

$$T_{ss1} * T_{s1sp} = T_{sp} = T_{cp} = \begin{pmatrix} -0.03 & 1.00 & 0.00 & -28.10 \\ -0.98 & -0.02 & -0.20 & 75.97 \\ -0.20 & -0.01 & 0.98 & -27.43 \\ 0.00 & 0.00 & 0.00 & 1.00 \end{pmatrix}$$

Equation 4.3: 4x4 transform matrix that defines the movement of probed points into the S or C reference frames of the surface model or CT scan.

$$T_{IC} = \begin{pmatrix} 1.00 & 0.03 & 0.09 & 1.99 \\ -0.01 & 0.99 & -0.17 & -20.82 \\ -0.10 & 0.17 & 0.98 & 42.46 \\ 0.00 & 0.00 & 0.00 & 1.00 \end{pmatrix}$$

Equation 4.4: Transform matrix generated by the NST UI during the planning phase. This matrix describes the positional offset between the glenoid implant and the center point of the CT scan.

Appendix C - Representing Probed Points in the I Reference Frame

To represent how we transferred the probed points through our reference frames, we will provide an example transformation using randomly selected sample point from one of the surgeons' trials to represent the ensemble.

The following point, p1, came directly out of the CMM machine:

$$\mathbf{p1} \rightarrow \mathbf{X= 80.23, Y = 34.23, Z = 128.39}$$

multiplying p1 by T_{SP}: p1*T_{SP} turns the coordinates above into the following coordinates representing the probed point in the S frame:

$$\mathbf{p1*T_{SP} \rightarrow X= 4.35, Y = -29.28, Z = 81.95,}$$

To bring these coordinates into frame I, we multiply these results by the inverse of T_{IC}.

$$\mathbf{p1*T_{IC}^{-1}*T_{SP} = p1*T_{IP} = X= -1.42, Y = -1.64, Z = 40.39.}$$

Hence, p1*T_{IP} turns the previous coordinates into

Appendix D - Python Script Used To Transform Points Through 4x4 Matrices

```
import numpy.matlib
import numpy as np

#This script will take points in the form of X,Y,Z array and transfer them through a 4x4
transform matrix to produce their new x,y,z coordinates after the repositioning.

#insert x,y,z points bellow as a numpy array.
input = np.array([[1.00214801,-22.20671,40.98697128]])

#below insert your 4x4 transform matrix as a numpy array
transform = np.array([[-0.025565355, -0.979220114, -0.201185381, 68.15234083],
[0.999671448, -0.024598001, -0.007305568, 29.76137362],
[0.002206405, -0.201305463, 0.979524952, 42.2186954],
[0, 0, 0, 1]])

def transformPoint(input, transform):
    output=np.zeros([input.shape[0],4])
    for n in range (input.shape[0]):
        inputRow = np.transpose(np.append(input[n,:], 1))
        output[n, ] = np.transpose(np.matmul(transform,inputRow))
    return output[:,0:3 ]

x= transformPoint(input, transform)
print (x)
```